Original Article

Integrating single-cell and bulk RNA sequencing to develop a cancer-associated fibroblast-related signature for immune infiltration prediction and prognosis in lung adenocarcinoma

Xiulin Huang[#], Hui Xiao[#], Yongxin Shi, Suqin Ben

Department of Respiratory and Critical Care Medicine, Shanghai General Hospital, Shanghai Jiao Tong University School of Medicine, Shanghai, China

Contributions: (I) Conception and design: X Huang, H Xiao; (II) Administrative support: S Ben; (III) Provision of study materials or patients: H Xiao; (IV) Collection and assembly of data: X Huang; (V) Data analysis and interpretation: Y Shi; (VI) Manuscript writing: All authors; (VII) Final approval of manuscript: All authors.

[#]These authors contributed equally to this work and should be considered as co-first authors.

Correspondence to: Suqin Ben. Department of Respiratory and Critical Care Medicine, Shanghai General Hospital, Shanghai Jiao Tong University School of Medicine, Shanghai, China. Email: bensuqin012@163.com.

Background: An accumulating amount of studies are highlighting the impacts of cancer-associated fibroblasts (CAFs) on the initiation, metastasis, invasion, and immune evasion of lung cancer. However, it is still unclear how to tailor treatment regimens based on the transcriptomic characteristics of CAFs in the tumor microenvironment of patients with lung cancer.

Methods: Our study examined single-cell RNA-sequencing data from the Gene Expression Omnibus (GEO) database to identify expression profiles for CAF marker genes and constructed a prognostic signature of lung adenocarcinoma using these genes in The Cancer Genome Atlas (TCGA) database. The signature was validated in 3 independent GEO cohorts. Univariate and multivariate analyses were used to confirm the clinical significance of the signature. Next, multiple differential gene enrichment analysis methods were used to explore the biological pathways related to the signature. Six algorithms were used to assess the relative proportion of infiltrating immune cells, and the relationship between the signature and immunotherapy response of lung adenocarcinoma (LUAD) was explored based on the tumor immune dysfunction and exclusion (TIDE) algorithm.

Results: The signature related to CAFs in this study showed good accuracy and predictive capacity. In all clinical subgroups, the high-risk patients had a poor prognosis. The univariate and multivariate analyses confirmed that the signature was an independent prognostic marker. Moreover, the signature was closely associated with particular biological pathways related to cell cycle, DNA replication, carcinogenesis, and immune response. The 6 algorithms used to assess the relative proportion of infiltrating immune cells indicated that a lower infiltration of immune cells in the tumor microenvironment was associated with high-risk scores. Importantly, we found a negative correlation between TIDE, exclusion score, and risk score.

Conclusions: Our study constructed a prognostic signature based on CAF marker genes useful for prognosis and immune infiltration estimation of lung adenocarcinoma. This tool could enhance therapy efficacy and allow individualized treatments.

Keywords: Single-cell RNA-sequencing; lung adenocarcinoma (LUAD); cancer-associated fibroblasts (CAFs); immune infiltration; prognostic signature

Submitted Feb 02, 2023. Accepted for publication Mar 17, 2023. Published online Mar 31, 2023.
doi: 10.21037/jtd-23-238
View this article at: https://dx.doi.org/10.21037/jtd-23-238

© Journal of Thoracic Disease. All rights reserved.

Introduction

Lung cancer is responsible for 18% of cancer-related mortality worldwide, making it the leading cause of death due to cancer (1). Based on histology, lung cancer is broadly divided into non-small cell lung cancer (NSCLC) and small-cell lung cancer (SCLC). Approximately 85% of lung cancer cases are NSCLCs, of which lung adenocarcinoma (LUAD) is the most common type (2). Over the last two decades, research into the understanding of the etiology and management of LUAD has made considerable progress, with targeted and immunotherapies providing a basis for the rational design of treatment regimens. However, most cancers develop resistance to targeted therapy, and only a fraction of patients with LUAD benefit from immunotherapies (3). Furthermore, the 5-year overall survival rate of patients with LUAD remains below 20% (4). Therefore, continued research into prognosis-related biomarkers of LUAD is required to predict treatment effects and improve outcomes.

A growing body of evidence suggests that the tumor microenvironment (TME) is essential in to dynamically orchestrating tumor initiation and progression (5). Moreover, the TME has a crucial impact on clinical outcomes and response to therapeutic interventions (5-7). Among the stromal cells in the TME, cancer-associated fibroblasts (CAFs) are the main cell type of the tumor mesenchyme, which not only play a critical role in promoting tumor invasion and metastasis but also contribute to regulating many immune components (8,9). On the one hand, CAFs exert a direct immunoregulatory effect through the secretome, which affects almost all cell types of innate and acquired immunity. On the other hand, CAFs induce uncontrolled extra matrix remodeling, indirectly disrupting immune cell infiltration into the tumor niche (10). Furthermore, CAFs may figure prominently in lung cancer development via crosstalk with cancer cells (11-14). A study found 11 genes in CAFs that were differentially expressed and associated with prognosis, using microarray gene expression analysis (15). This indicates that changes in oncogenes or tumor suppressor genes in CAFs may have a close relationship with tumor development. Numerous studies indicate that the survival rates of various malignancies are associated with the histological features of CAFs. CAFs are correlated with poor outcomes in patients with LUAD and contribute to therapy resistance (13,16,17). In the case of colorectal cancer, previous research has linked CAFs and pro-fibroblastic responses with an unfavorable prognosis. However, another independent study found that the pro-fibroplastic type, a histologic subtype in CAFs, was a predictor of good prognosis in colorectal cancer (18). Given the roles of CAFs in tumor progression and treatment response, it is worth developing a CAF-related gene signature for LUAD and evaluating its associations with prognosis and the immune infiltration characteristics in the TME.

Recently, the TME has been extensively analyzed through single-cell RNA-sequencing (scRNA-seq). This still emerging technique allows for a finer characterization of tumor, adjacent stromal, and infiltrating immune cells (19,20). Compared with conventional transcriptomic investigation, scRNA-seq can identify specific cell types of the TME, discern the gene expression patterns of each cell, and provides clear insights into the whole tumor ensemble, thus enabling the characterization of various cell types and the identification of marker genes (21,22). Song *et al.* constructed a 9-gene signature for predicting LUAD prognosis based on 258 B-cell marker genes identified with scRNA-seq analysis, and the signature can serve as a predictor of immunotherapy (23).

In this study, we used scRNA-seq data of LUAD samples from the Gene Expression Omnibus (GEO) database to derive a cluster of CAFs and identify their marker genes. We then developed a prognostic signature based on these

Highlight box

Key findings

- We constructed a novel signature based on the cancer-associated fibroblasts marker genes. The novel prognostic signature had powerful predictive capability for the out-comes of patients with lung adenocarcinoma. Importantly, it was closely correlated with oncogenic signaling pathways and immune infiltration status of the tumor mi-croenvironment.

What is known and what is new?

- Lung cancer is one of the most commonly diagnosed cancers. CAFs can have an im-portant impact on lung carcinogenesis, metastasis, invasion, and immune evasion.
- We constructed and validated a prognostic signature based on 11 CAF marker genes via integration of single cell RNA-sequencing (scRNA-seq) and bulk RNA-sequencing analysis, which was useful for prognosis and estimation of immune infil-tration in LUAD.

What is the implication, and what should change now?

- We developed a biomarker-based prognostic tool to predict outcome and immuno-therapy impact which may facilitate individualized treatment and improved progno-sis. However, the predictive power of this tool should be evaluated in large, prospective clinical studies.

© Journal of Thoracic Disease. All rights reserved.

CAF marker genes through bulk RNA-seq analysis. Finally, we validated the prediction potential of the signature in 3 GEO cohorts and assessed the prognostic significance by investigating the variation of enriched biological signal pathways, immune cell infiltration characteristics, and immunotherapy response in patients with LUAD with different risk scores. As a result, we found the signature to be closely correlated with oncogenic signaling pathways and the immune infiltration status of the TME, which in turn may influence the clinical outcomes of patients and the response to immunotherapy. We present the following article in accordance with the TRIPOD reporting checklist (available at https://jtd.amegroups.com/article/view/10.21037/jtd-23-238/rc).

Methods

Data source and preprocessing

We downloaded scRNA sequencing data (GSE149655) from the National Center for Biotechnology Information (NCBI) GEO database (https://www.ncbi.nlm.nih.gov/geo/). We downloaded the transcriptome expression profiles of LUAD and matched clinical information from The Cancer Genome Atlas database (TCGA; http://cancergenome.nih.gov/) and GEO database. TCGA database contained 527 LUAD samples and 59 non-LUAD samples. We normalized RNA-seq data to transcripts per million data and then performed $\log_2$ conversion. To perform a joint analysis of smooth RNA-seq and clinical data, we removed samples with incomplete clinical information. Ultimately, 500 LUAD samples from TCGA served as the training set. We used the other LUAD samples from the GEO database, including GSE30219 (n=85), GSE31210 (n=226), and GSE72094 (n=398) for further validation. The study was conducted in accordance with the Declaration of Helsinki (as revised in 2013).

Determining the prognosis value of the CAF proportion

We estimated the proportion of CAFs in the samples from the GEO and TCGA data using the EPIC algorithm via the "EPIC" R package (The R Foundation for Statistical Computing). EPIC is one of the tools that calculates the percentage of different cell types in the TME based on RNA-seq data (24). We separated the LUAD samples into a high CAF proportion and a low CAF proportion group based on the optimal cutoff according to the "survminer" R package. To evaluate the prognosis value of the CAF proportion, we conducted a survival analysis using the "survival" and "survminer" R packages. Additionally, we assessed the activity, infiltration levels, and immune-related functions of 19 immune cells through single-sample gene set enrichment analysis (ssGSEA) using the "GSEABase" and "GSVA" R packages (25). Finally, we analyzed the correlations between CAF proportion and the infiltration level of different immune cells or functions using the Wilcoxon test. For all these analyses, we considered $P<0.05$ to indicate a significant difference.

Identification of CAF marker genes using scRNA-seq analysis

We analyzed scRNA-seq data using the "Seurat" (version 4.0.5) and "SingleR" (version 1.6.1) packages in R software (26,27). We removed the cells with mitochondrial gene content above 5% and mapped genes below 50. We also removed cell clusters with fewer than 3 cells. Next, we conducted principal component analysis (PCA) on the top 2,000 variable expression genes. We applied the t-distributed stochastic neighbor embedding (tSNE) algorithm to visualize the results. Finally, we performed a differential analysis between fibroblasts and other cell types. Based on the differential analysis, we considered genes showing significantly higher expression in fibroblasts as CAF marker genes [$\log_2$ fold change (FC) >1 and $P<0.05$].

Development and validation of a prognostic signature related to CAFs

To find CAF marker genes with significantly different expression levels in LUAD samples and non-LUAD samples, we performed a differential analysis on TCGA data set (using the "limma" R package) with a cutoff of $|\log_2(FC)| > 1$ and $P<0.05$ (28). To investigate the prognostic CAF marker genes, we performed univariate Cox regression analyses among differentially expressed CAF marker genes using the "survival" R package. We visualized the results as a forest map using the "forestplot" R package. Subsequently, we conducted least absolute shrinkage and selection operator (LASSO) Cox regression analysis to further reduce the number of variables in the model and construct a signature related to the prognostic CAF marker genes with the following formula:

© Journal of Thoracic Disease. All rights reserved.

$$\begin{aligned} Risk\ score = {} & \left(0.044 \times AKAP12\ expression\right) + \left(-0.047 \times FMO3\ expression\right) \\ & + \left(0.123 \times KRT8\ expression\right) + \left(0.050 \times FSTL3\ expression\right) \\ & + \left(-0.016 \times BMP5\ expression\right) + \left(-0.008 \times IGHM\ expression\right) \\ & + \left(-0.014 \times SFTPB\ expression\right) \\ & + \left(-0.042 \times TMEM125\ expression\right) \\ & + \left(-0.021 \times CYP4B1\ expression\right) + \left(0.007 \times ID1\ expression\right) \\ & + \left(-0.001 \times IRX2\ expression\right) \end{aligned} \quad [1]$$

All the LUAD samples in the GEO and TCGA data sets were separated into a high-risk group and a low-risk group based on the median risk score.

We assessed the overall survival prediction ability of the signature using Kaplan-Meier survival curves, receiver operating characteristic (ROC) curves, and risk curves using the "survminer", "timeROC", and "pheatmap" R packages. We further used tSNE and PCA to determine the distribution of different risk groups and estimate the classification ability via the "Rtsne" R package. We also confirmed the overall survival prediction ability of the signature via Kaplan-Meier survival analysis, ROC analysis, risk scatter plot, tSNE, and PCA on the GSE30219, GSE31210, and GSE72094 data sets.

Investigation of the clinical significance of the CAF-related prognostic signature

To investigate whether the risk score is an independent prognostic factor, we performed univariate and multivariate Cox regression analysis on TCGA, GSE30219, GSE31210, and GSE7094 data sets. Next, we visualized these results as a forest map. Additionally, we verified the relationship between risk score and clinicopathological parameters in LUAD samples via the Kruskal-Wallis or Wilcoxon test and visualized the results as box violin plots.

Function and pathway enrichment analysis of the different risk groups

Based on the study of Xiao *et al.* (29), we established the signature of 5 well-known cancer-related pathways (Table S1), including the cell cycle, Hippo, Myc, Notch, and PI3K pathways, and calculated an enrichment score for each pathway in each LUAD sample with the ssGSEA method. Using the Wilcoxon test, we analyzed the correlation between the pathway enrichment score and risk. Using the "clusterProfiler" R package, we performed gene ontology (GO) enrichment (30). In the results, we focused on GO terms with an adjusted P value <0.01, and to avoid very general terms, we limited the final GO terms lists to the set of pathways with fewer than 300 genes examined for annotation. Meanwhile, we evaluated the similarity between the GO terms using the "GOSemSim" R package and clustered the GO terms by similarity visualized as a tree diagram (using the "ggtree" R package). We obtained 50 gene sets of hallmark pathways described in the molecular signature database (MsigDB database; http://software.broadinstitute.org/gsea/msigdb) via the "msigdbr" R package. To reduce pathway overlap and redundancies, we pruned each pathway-related gene set to keep unique genes and remove all genes related to 2 or more pathways. Subsequently, we performed gene set variation analysis (GSVA) to calculate the enrichment score of each pathway for every LUAD sample via the "GSVA" R package. Next, we performed differential analysis with the "limma" R package to identify the correlation between enrichment scores of hallmark pathways and risk groups and visualize the difference of the pathways with an adjusted P value <0.05 as a heatmap using the "pheatmap" R package. Finally, we conducted GSEA to calculate the enrichment score of Kyoto Encyclopedia of Genes and Genomes (KEGG; http://www.genome.jp/kegg) pathways using the "clusterProfiler" R package.

Evaluation of TME immunological characteristics in LUAD

We used the CIBERSORT, EPIC, MCP-counter, quanTIseq, TIMER, and xCell algorithms to calculate the infiltration level of immune cells in the TME of LUAD (24,31-35). Additionally, we used the Wilcoxon test to assess the association between the infiltration level of immune cells and risk level. We selected the immune cells with P<0.0001 and visualized them as a heatmap. Next, we downloaded hematoxylin and eosin (HE)-stained images of TCGA-LUAD samples from the Genomic Data Commons (GDC; https://portal.gdc.cancer.gov/) and obtained matched immunophenotype pathology of TCGA-LUAD samples from the supplementary research materials of Saltz *et al.* (36). Additionally, we obtained the list of 129 immunomodulators (Table S2), including chemokines, interleukin, interferons, receptors, and other cytokines from the study of Charoentong *et al.* (37). The tumor immune dysfunction and exclusion algorithm (TIDE; http://tide.dfci.harvard.edu) by Jiang *et al.* is based on the combination and modeling of data from 189 human malignant studies. The TIDE score can be used to assess the clinical response to immunotherapy (38). We thus used the TIDE algorithm

© Journal of Thoracic Disease. All rights reserved.

to calculate the TIDE score of TCGA-LUAD samples and investigated the correlation between the efficacy of immunotherapy and risk score using the Wilcoxon test.

Statistical analysis

We used R software (version 4.1.0) and various R packages to analyze the data and visualize the results. For all analyses, statistical significance was defined as $P<0.05$.

Results

The clinical significance of the CAF proportion in LUAD

First, we analyzed the clinical significance of the CAF proportion in LUAD. We divided the patients into 2 groups (high CAF and low CAF proportions) according to the optimal cutoff points. Patients with a higher CAF proportion had poor overall survival (GSE30219, GSE31210, and GSE72094; *Figure 1A-1C*). Moreover, the high CAF groups had lower overall survival rates than did the low CAF groups in TCGA and GSE13213 cohorts, albeit not significantly (P=0.06 and P=0.089; *Figure 1D,1E*), and poor disease-free survival (GSE31210; *Figure 1F*). Additionally, the 2 groups differed significantly in immune cell infiltration and immune-related pathway activation, indicating a potential association between the CAF proportion and immune function in LUAD patients (*Figure 1G*). Taken together, these results suggest that a high CAF proportion was a potential risk factor for LUAD.

Identification of marker genes associated with CAFs

The screening yielded gene expression profiles for 1546 cells that we used for subsequent analysis from 2 LUAD samples. We performed PCA using the 2000 variable genes to reduce the dimensionality and classify cells into 14 clusters. Subsequently, we adopted tSNE analysis to visualize the results (*Figure 2A*). We annotated each cell cluster by cross-referencing the differentially expressed genes (DEGs) with the well-known marker genes for each cluster. The following cell types were described: epithelial cells, endothelial cells, fibroblasts, T cells, macrophages, and tissue stem cells (*Figure 2B*). In addition, we identified significant differential marker genes of each cluster using $\log_2$ FC >1 and $P<0.05$ as thresholds. *Figure 2C* displays the heatmap for the top 10 significantly expressed marker genes of 6 cell clusters. Ultimately, we screened 417 CAF marker genes in LUAD.

Development and validation of the CAF-related gene signature

In the process of developing a prognostic signature based on CAF marker genes in LUAD, we used TCGA data as a training cohort. We first screened 232 DEGs (47 upregulated and 185 downregulated), using $P<0.05$ and $|\log_2(FC)| >1$ as thresholds (*Figure 3A*). Next, we performed univariate Cox regression analysis. We identified 81 CAF marker genes distinctly associated with prognostication (Figure S1). We then carried out a LASSO and Cox regression analysis on these genes to select the most valuable ones for prognosis, resulting in a model containing 11 genes: *AKAP12*, *FMO3*, *KRT8*, *FSTL3*, *BMP5*, *IGHM*, *SFTPB*, *TMEM125*, *CYP4B1*, *ID1*, and *IRX2* (*Figure 3B*). Next, we calculated each patient's risk score according to Eq. [1].

Figure 3C presents the patients' survival times and risk score distribution. The Kaplan-Meier curve revealed greater survival in low-risk patients with LUAD than in high-risk patients with LUAD in TCGA data set (*Figure 3D*). To assess the accuracy of the signature, we generated ROC curves for overall survival prediction at 1, 3, and 5 years, which yielded respective area under the ROC curve (AUC) values of 0.698, 0.695, and 0.651 (*Figure 3E*). *Figure 3F,3G* present the PCA and tSNE results. Patients with LUAD were separated into high-risk and low-risk groups according to risk score. Next, we divided the patients into subgroups based on clinical characteristics and performed a Kaplan-Meier analysis for each group. The predictive capacity of the signature was further verified in subgroups of different ages, genders, and stages. In all clinical subgroups, the high-risk patients had a poor prognosis ($P<0.0001$; Figure S2), demonstrating the powerful predictive ability of this prognostic signature.

To further validate the robustness of the CAF-related signature, we assessed its prediction power in 3 independent cohorts (GSE30219, GSE31210 and GSE72094). We calculated the risk scores of samples in each validation data set using the same formula and divided the patients with LUAD into high- and low-risk groups based on the median value. *Figure 4A-4C* show the distribution of risk scores in the validation data sets, and samples in the high-risk group had poor outcomes. In line with the training cohort, the Kaplan-Meier survival curves revealed that the low-risk group had a superior survival to the high-risk group (*Figure 4D-4F*). *Figure 4G-4I* present each cohort's ROC curves and AUCs. Thus, the prognostic signature had a good prediction ability. Furthermore, the PCA and

© Journal of Thoracic Disease. All rights reserved.

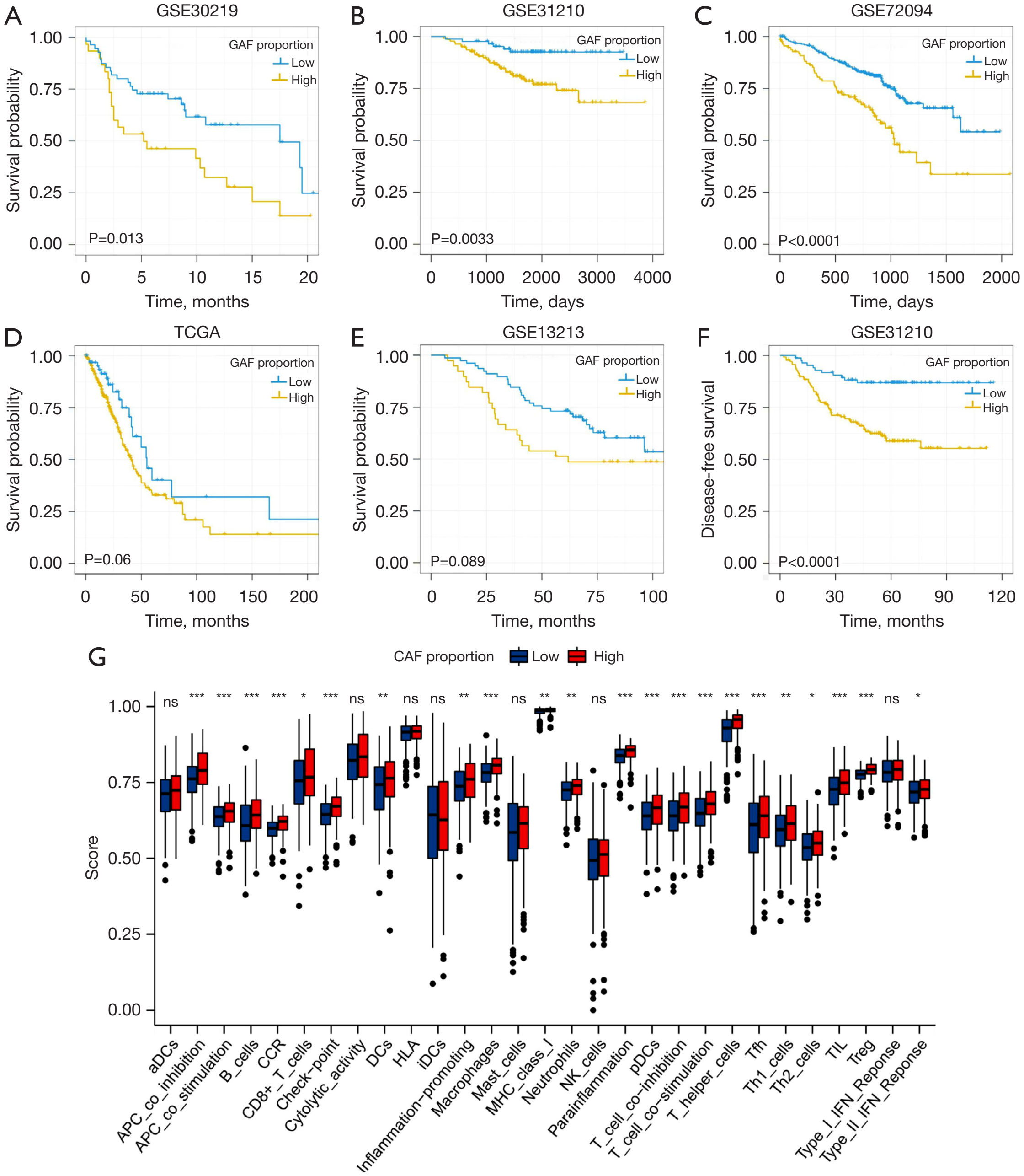

Figure 1 Clinical significance of the CAF proportion in patients with LUAD. (A-E) Kaplan–Meier curves of overall survival analysis for the high- and low-CAF proportion groups in the GSE30219, GSE31210, GSE72094, TCGA, and GSE13213 cohorts. (F) Kaplan-Meier disease-free survival curves for the high- and low-CAF proportion groups in GSE31210. (G) Comparison of immune cell infiltration and immune-related pathways between the high- and low-CAF proportion groups. ns, P≥0.05; *, P<0.05; **, P<0.01; ***, P>0.001. CAF, cancer-associated fibroblast; LUAD, lung adenocarcinoma; TCGA, The Cancer Genome Atlas; aDCs, activated dendritic cells; APC, antigen-presenting cells; CCR, chemokine receptors; HLA, human leukocyte antigen; iDCs, immature dendritic cells; MHC, major histocompatibility complex; NK cells, natural killer cells; pDCs, plasmacytoid dendritic cells; TIL, tumor infiltrating lymphocyte; IFN, interferon; GAF, Global Assessment of Functioning.

© Journal of Thoracic Disease. All rights reserved.

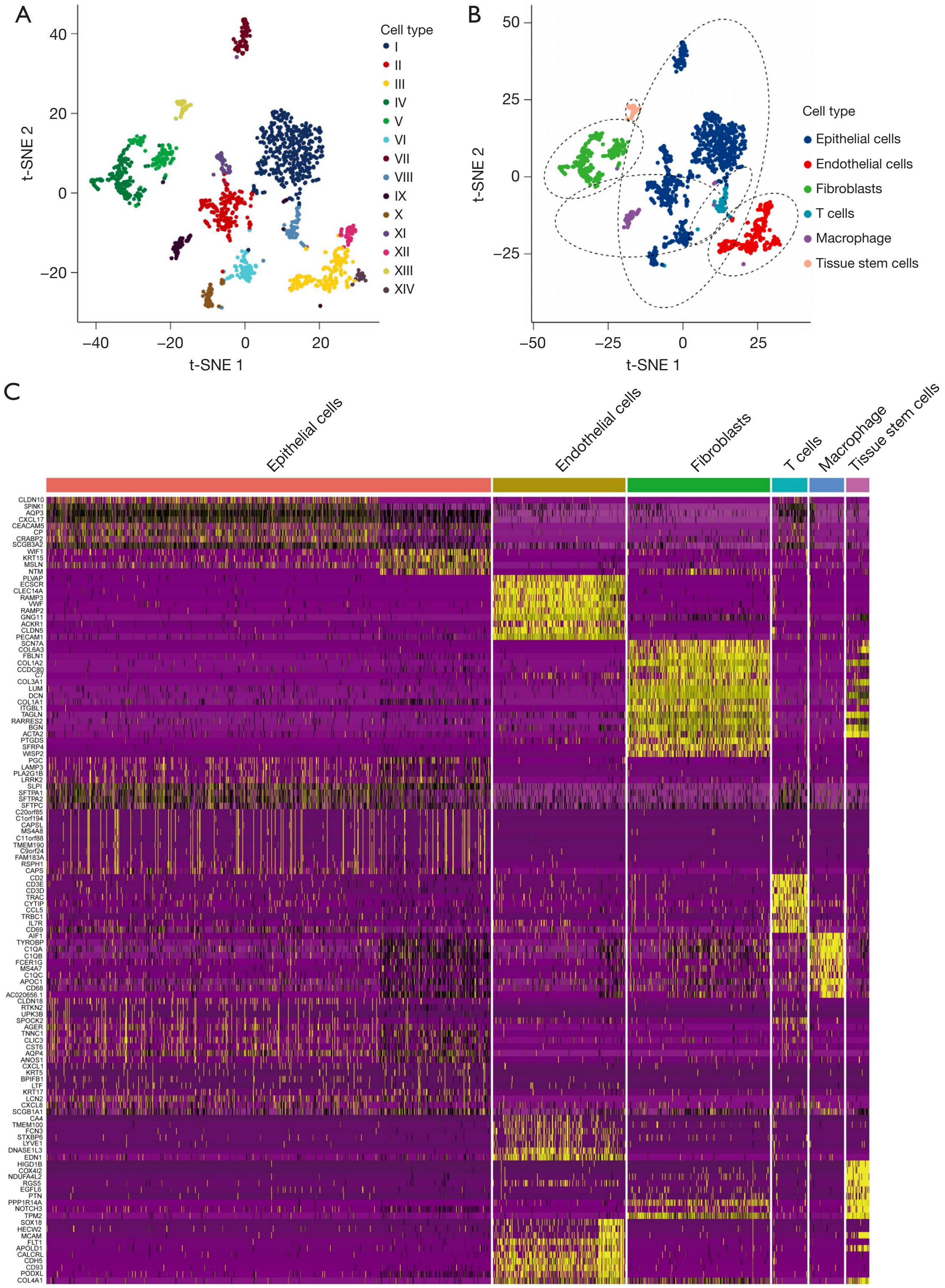

Figure 2 Identification of CAF marker genes in LUAD with single-cell RNA-sequencing. (A) tSNE plot colored by cell population; (B) cell clusters identified with marker genes for each cell type; (C) heatmap showing the top 10 significantly expressed marker genes in 6 cell clusters. CAF, cancer-associated fibroblast; LUAD, lung adenocarcinoma; tSNE, t-distributed stochastic neighbor embedding.

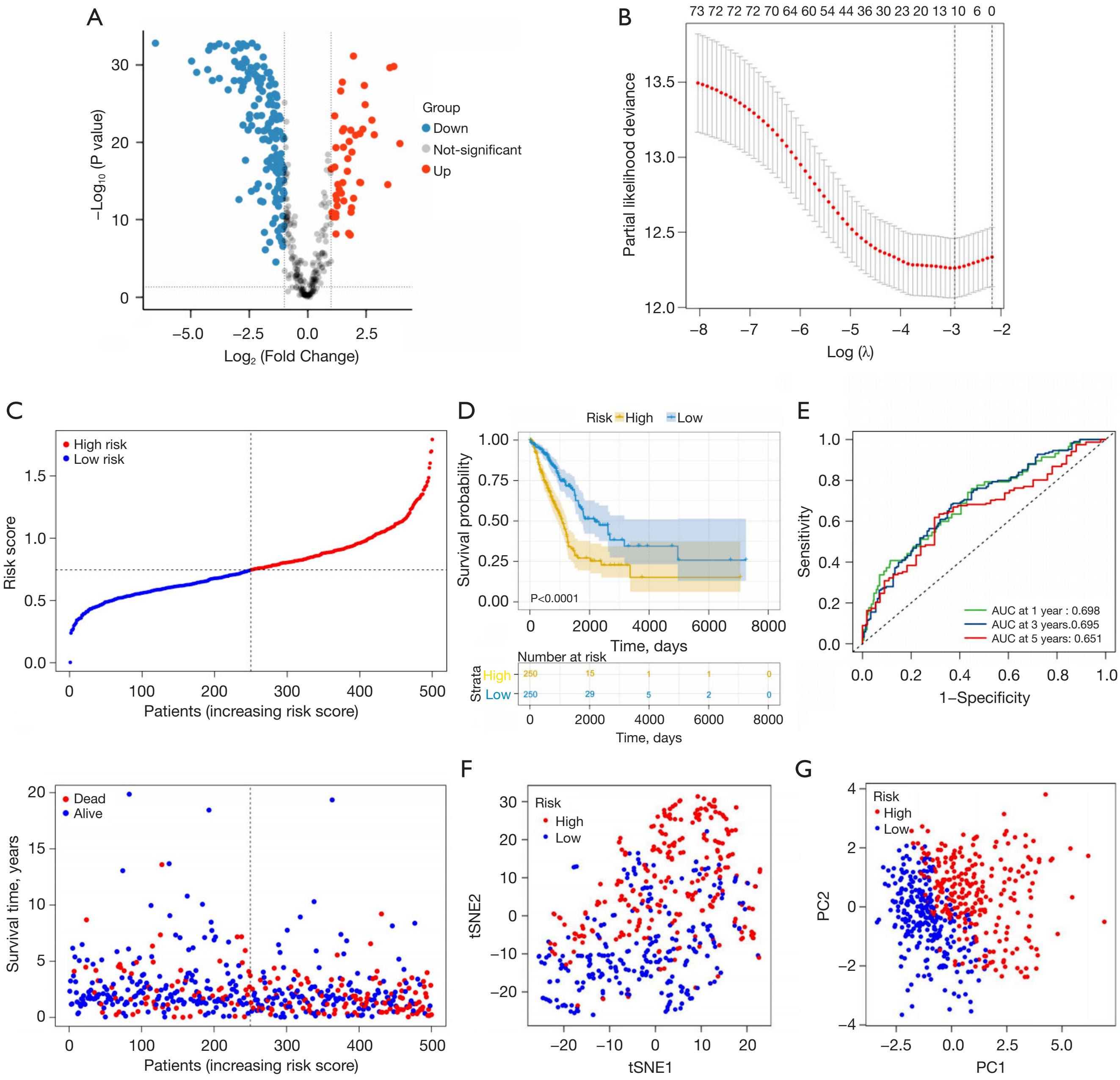

Figure 3 Construction of the prognostic model based on CAF marker genes in TCGA database. (A) Volcano plot exhibiting the DEGs between lung cancer and normal tissues. (B) Selection of the λ in the LASSO model through 10-fold cross-validation. (C) Distribution of risk scores and patients' survival times. (D) Kaplan-Meier overall survival curves in the high- and low-risk groups. (E) ROC curves for predicting mortality risk at 1, 3, and 5 years. (F) The tSNE analysis. (G) The PCA analysis. CAF, cancer-associated fibroblast; TCGA, The Cancer Genome Atlas; DEGs, differentially expressed genes; LASSO, least absolute shrinkage and selection operator; ROC, receiver operating characteristic; tSNE, t-distributed stochastic neighbor embedding; PCA, principal component analysis.

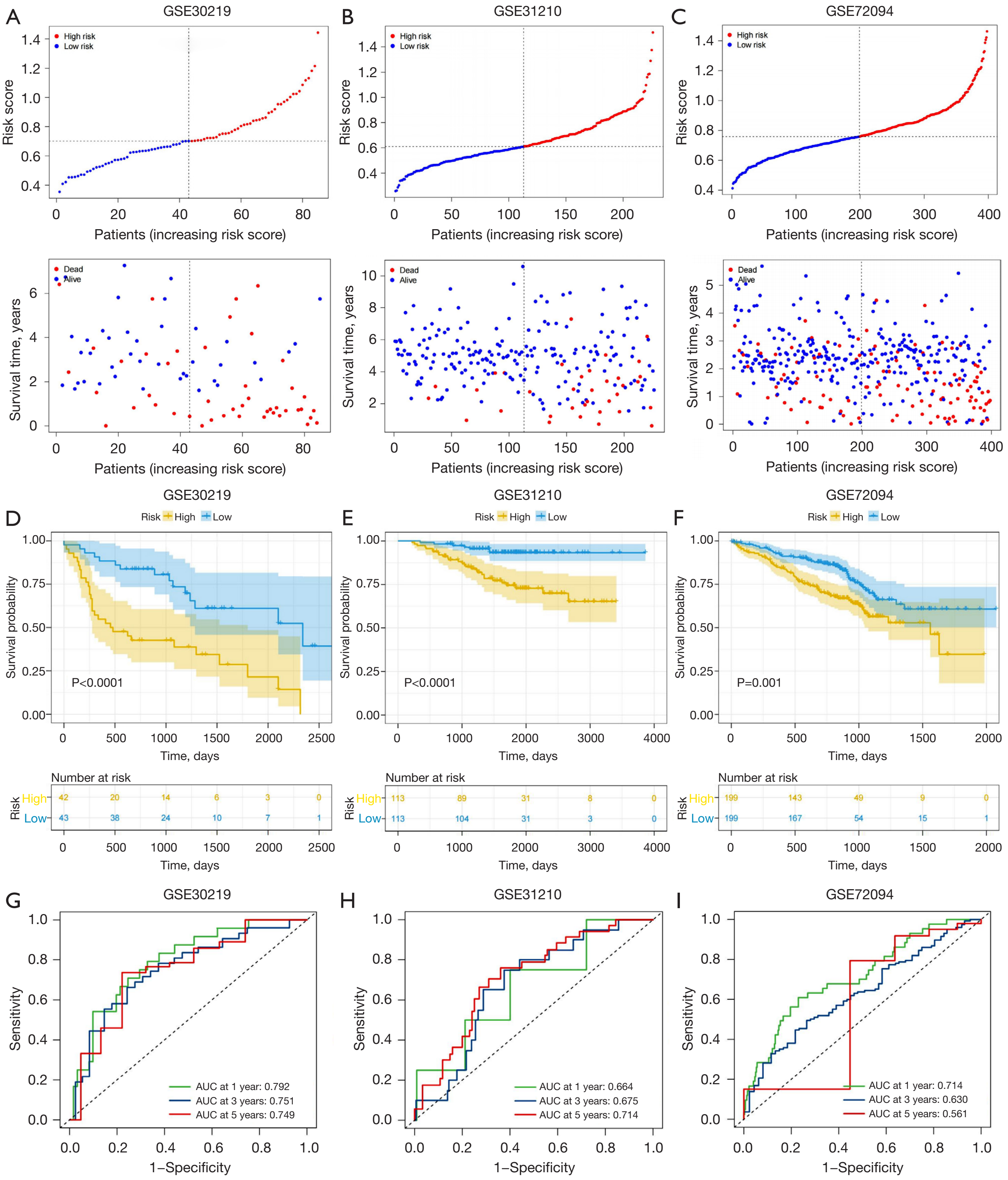

Figure 4 Prognostic signature validation in the 3 independent GEO cohorts. (A-C) Risk scores and survival status in the different cohorts. (D-F) Kaplan-Meier analysis of the overall survival in patients with LUAD in the 3 data sets. (G-I) Validation cohort ROC curves for overall survival at 1, 3, and 5 years. GEO, the Gene Expression Omnibus; AUC, area under curve; LUAD, lung adenocarcinoma; ROC, receiver operating characteristic.

© Journal of Thoracic Disease. All rights reserved.

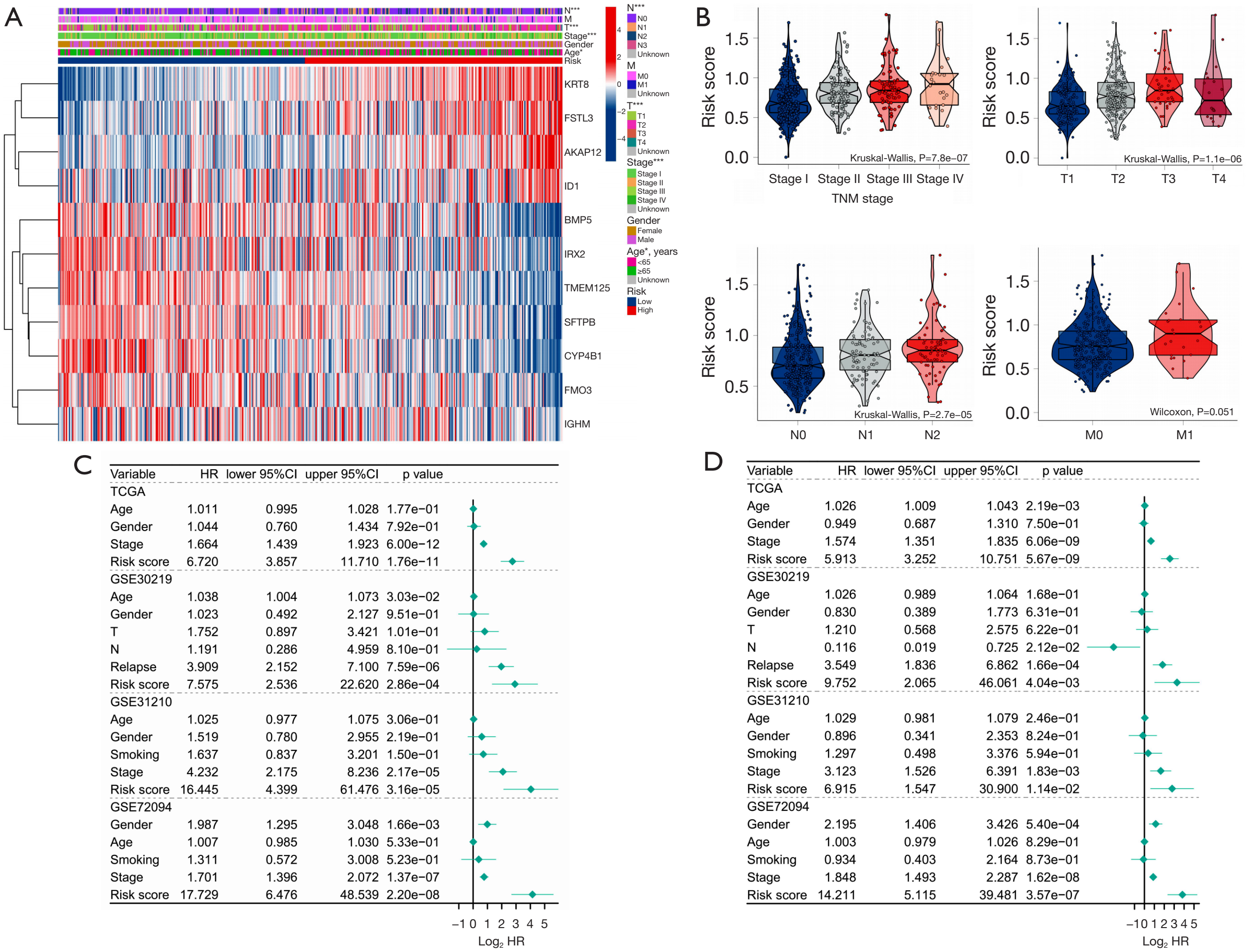

C

Variable	HR	lower 95%CI	upper 95%CI	p value
TCGA				
Age	1.011	0.995	1.028	1.77e−01
Gender	1.044	0.760	1.434	7.92e−01
Stage	1.664	1.439	1.923	6.00e−12
Risk score	6.720	3.857	11.710	1.76e−11
GSE30219				
Age	1.038	1.004	1.073	3.03e−02
Gender	1.023	0.492	2.127	9.51e−01
T	1.752	0.897	3.421	1.01e−01
N	1.191	0.286	4.959	8.10e−01
Relapse	3.909	2.152	7.100	7.59e−06
Risk score	7.575	2.536	22.620	2.86e−04
GSE31210				
Age	1.025	0.977	1.075	3.06e−01
Gender	1.519	0.780	2.955	2.19e−01
Smoking	1.637	0.837	3.201	1.50e−01
Stage	4.232	2.175	8.236	2.17e−05
Risk score	16.445	4.399	61.476	3.16e−05
GSE72094				
Gender	1.987	1.295	3.048	1.66e−03
Age	1.007	0.985	1.030	5.33e−01
Smoking	1.311	0.572	3.008	5.23e−01
Stage	1.701	1.396	2.072	1.37e−07
Risk score	17.729	6.476	48.539	2.20e−08

D

Variable	HR	lower 95%CI	upper 95%CI	p value
TCGA				
Age	1.026	1.009	1.043	2.19e−03
Gender	0.949	0.687	1.310	7.50e−01
Stage	1.574	1.351	1.835	6.06e−09
Risk score	5.913	3.252	10.751	5.67e−09
GSE30219				
Age	1.026	0.989	1.064	1.68e−01
Gender	0.830	0.389	1.773	6.31e−01
T	1.210	0.568	2.575	6.22e−01
N	0.116	0.019	0.725	2.12e−02
Relapse	3.549	1.836	6.862	1.66e−04
Risk score	9.752	2.065	46.061	4.04e−03
GSE31210				
Age	1.029	0.981	1.079	2.46e−01
Gender	0.896	0.341	2.353	8.24e−01
Smoking	1.297	0.498	3.376	5.94e−01
Stage	3.123	1.526	6.391	1.83e−03
Risk score	6.915	1.547	30.900	1.14e−02
GSE72094				
Gender	2.195	1.406	3.426	5.40e−04
Age	1.003	0.979	1.026	8.29e−01
Smoking	0.934	0.403	2.164	8.73e−01
Stage	1.848	1.493	2.287	1.62e−08
Risk score	14.211	5.115	39.481	3.57e−07

Figure 5 Clinical relevance of the CAF-related signature in TCGA LUAD cohort. (A) Heat map of the expression differences of 11 genes in the different risk groups of TCGA cohort annotated by clinical characteristics. (B) Comparison of risk scores in patients with lung cancer of TCGA cohort at different clinical stages (T stage, N stage, and M stage). (C,D) Forest maps of the univariate and multivariate Cox regression analysis for the risk score and other clinical characteristics in the training set. *, P<0.05; ***, P<0.001. CAF, cancer-associated fibroblast; TCGA, The Cancer Genome Atlas; LUAD, lung adenocarcinoma.

tSNE allowed the clear distinction of the samples in each cohort (Figure S3). Moreover, we also classified the patients in the GSE31210 and GSE72094 cohorts into different subgroups based on their clinical variables. The Kaplan-Meier overall survival analysis revealed that low-risk scores were associated with better outcomes (Figure S4).

Clinical significance of the prognostic signature in LUAD

Our next step was to evaluate the correlation between this signature and clinical features, such as disease stage, in LUAD patients of the TCGA cohort. Based on the median risk score, we categorized the training cohort patients into high-risk and low-risk groups and produced a heatmap of the gene expression levels (*Figure 5A*). The scores significantly increased as LUAD stages progressed (*Figure 5A,5B*). These outcomes revealed that the CAF-related signature and the clinicopathological parameters of patients with LUAD were correlated and confirmed the clinical application value of the prognostic model. We additionally performed 2-step Cox regression analyses (univariate and multivariate) to confirm whether the risk scores were independent of other clinical characteristics, such as age, gender, and stage, in predicting prognosis. As expected,

© Journal of Thoracic Disease. All rights reserved.

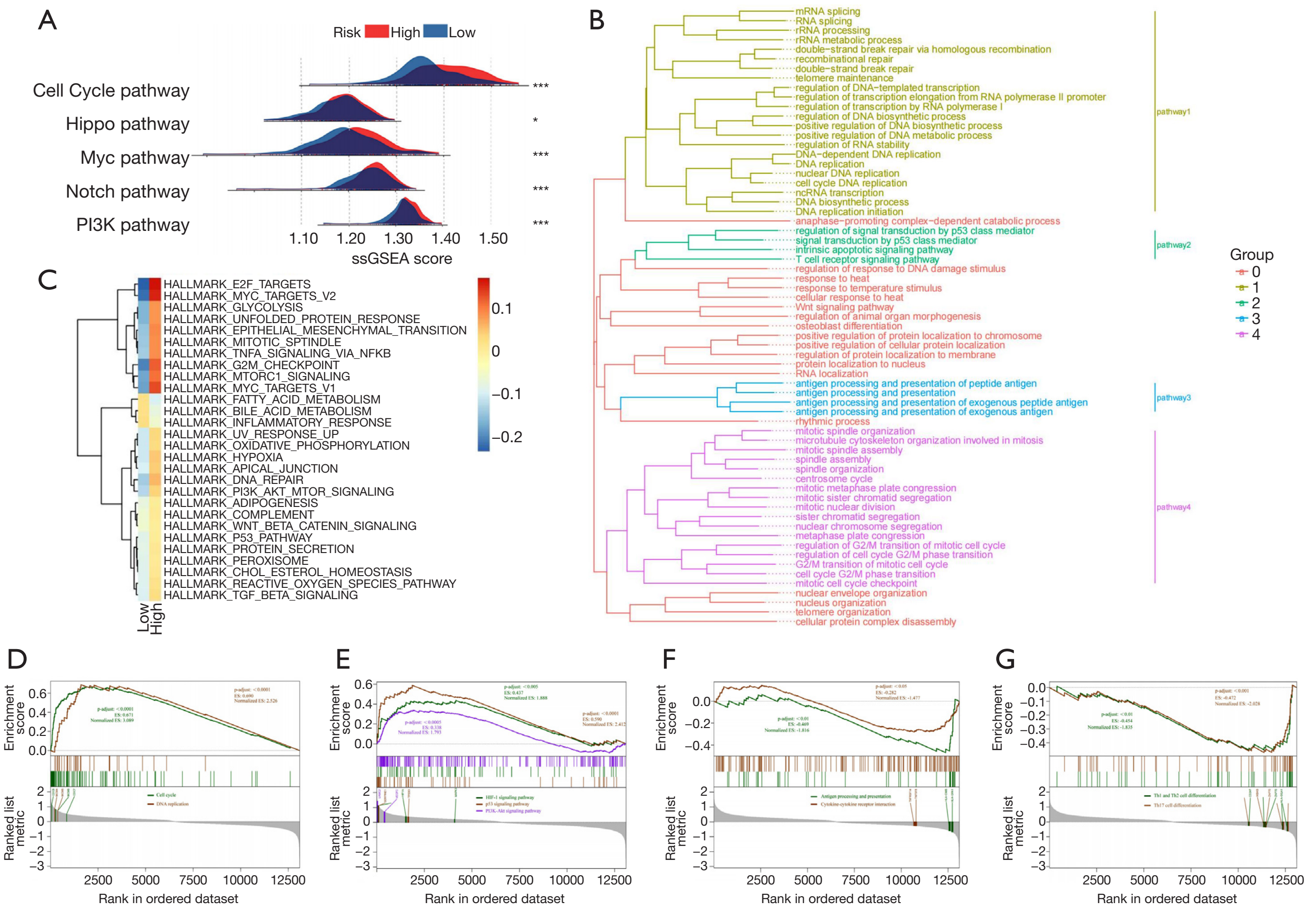

Figure 6 Analysis of the differentially associated signaling pathways between the high-risk and low-risk groups in TCGA cohort. (A) Mountain map showing the score variations in 5 oncogenic pathways between the 2 groups (Wilcoxon test). *, P<0.05; ***, P<0.001. (B) GO enrichment analysis of the DEGs between the high- and low-risk groups, grouped by functional themes. (C) The different statuses of the signaling pathways between the different groups according to GSVA enrichment analysis. (D-G) The status of biological pathways in the high-risk group according to GSEA. TCGA, The Cancer Genome Atlas; GO, Gene Ontology; DEGs, differentially expressed genes; GSVA, gene set variation analysis; ssGSEA, single-sample gene set enrichment analysis; ES, enrichment score.

the results from TCGA data set [hazard ratio (HR) =5.913, 95% confidence interval (CI): 3.252–10.751; P=5.67×10^{-9}] and the other 3 cohorts (GSE30219: HR =9.752, 95% CI: 2.065–46.061, P=4.04×10^{-3}; GSE31210: HR =6.915, 95% CI: 1.547–30.900, P=1.14×10^{-2}; GSE72094: HR =14.211, 95% CI: 5.115–39.481, P=3.57×10^{-7}) demonstrated that the risk score was an independent prognostic factor for LUAD (*Figure 5C,5D*). Overall, these results support the potential clinical utility of the prognostic model.

Signal differences between the risk groups

We identified the DEGs between the high-risk and low-risk groups and identified the features of the related signaling pathways. We used the ssGSEA analysis scores derived using the published signature correlated to 5 frequent oncogenic signaling pathways, including the cell cycle, Hippo, Myc, Notch, and PI3K pathways, to compare the 2 groups (29). We found that the pathways had higher levels in the high-risk group (*Figure 6A*). Then, we assessed the correlation between these pathways and the 11 CAF marker genes. Among them, *AKAP12*, *FSTL3*, *ID1*, and *KRT8* were positively correlated with the carcinogen pathways (Figure S5). Moreover, we conducted GO enrichment analysis on these DEGs and grouped them according to functional theme. The analysis revealed that these genes

© Journal of Thoracic Disease. All rights reserved.

were related to antigen processing and presentation, cell cycle, p53 signaling, T-cell receptor signaling, and regulation of genetic material pathways (*Figure 6B*). Through functional enrichment analysis, we found that the high-risk group had upregulated levels of cancer- and cell cycle–related gene sets, with terms including "SHEDDEN LUNG CANCER POOR SURVIVAL A6", "GOBP CELL DIVISION", and "GOBP MITOTIC CELL CYCLE PROCESS" (Figure S6). Meanwhile, the high-risk group had downregulated levels of gene sets correlated to immune response, with terms including "GOBP ANTIGEN BINDING" and "GOBP ADAPTIVE IMMUNE RESPONSE".

Similarly, the GSVA revealed that the high-risk group had a prevalence of cell cycle and common carcinogen pathways, including terms "MITOTIC SPINDLE", "G2M CHECKPOINT", "MYC TARGETS", "PI3K AKT MTOR SIGNALING", "WNT BETA CATENIN SIGNALING", and "TGF BETA SIGNALING" (*Figure 6C*). Furthermore, the inflammatory pathway termed "INFLAMMATORY RESPONSE" was inhibited in the high-risk group, indicating immunosuppression, which was consistent with our expectations. Figure S7 presents the association between the CAF marker genes and these signaling pathways as a heatmap. The GSEA also confirmed that cell cycle and PI3K-Akt signaling pathways were activated in the high-risk group (*Figure 6D,6E*). Antigen processing and presentation; cytokine-cytokine receptor interaction; and T helper (Th)1, Th2-, and Th17-cell differentiation was significantly inhibited in the high-risk group (*Figure 6F,6G*). These results suggest that the prognostic signature was positively correlated with tumor progression-related pathways and negatively associated with immune-related pathways, further demonstrating the value of the signature in predicting clinical outcomes of patients with LUAD.

Correlation between TME immune cell infiltration characteristics and the CAF marker genes

Given the pivotal role of CAFs in the immune regulation of the TME and the association of the prognostic signature with immune-related biological pathways, we next investigated the relationship between the signature and immune cell infiltration in LUAD. We first used the CIBERSORT, EPIC, MCP-counter, quanTIseq, TIMER, and xCell algorithms to assess the proportion of immune cells infiltrating LUAD samples. Most immune cells with antitumor activity, including $CD8^+$ T cells, B cells, monocytes, neutrophils, and myeloid dendric cells, had higher levels of infiltration in the low-risk group (*Figure 7A*). We next identified the relationships between the prognostic signature and the immune cells. We found that most immune cells expressed negative correlations with the 4 genes included in the signature (*AKAP12*, *KRT8*, *FSTL3*, and *ID1*), which are detrimental to the prognosis of patients with LUAD (Figure S8A). Additionally, immune cell components were positively correlated with the other 7 prognostically favorable genes, consistent with our expectations.

To further explore the correlation between the model and the immune cell infiltration of TME, we used the ESTIMATE algorithm to compare the immune and matrix components in the TME of LUAD. The high-risk group had higher tumor purity but a lower immune score and ESTIMATE score than did the low-risk group (Figure S8B-S8E). These results confirmed the negative correlations between the abundance of immune cell infiltration in the TME and the risk score. Furthermore, we downloaded the pathology slide and compared the levels of immune cell infiltration in the tumor tissue of patients with different risk scores from TCGA data set. Surprisingly, low-risk patients had a higher infiltration of immune cells in their tumor nests (*Figure 7B*, Figure S9). Moreover, using on the tumor-infiltrating lymphocyte map of TCGA HE pathology slides published by Saltz *et al.*, we compared the discrepancy in infiltrating lymphocytes between patients with different risk scores and found higher levels of lymphocyte infiltration in patients with higher risk scores (36). Given that chemokines are crucial TME components, we analyzed the levels of chemokine mRNA expression in TCGA cohort. Higher chemokine abundance was associated with favorable lung cancer prognoses, with chemokines, including CCL17, CCR2, and CCR4, being more abundant in the low-risk group (*Figure 7C*). Furthermore, considering the impact of tumor immune infiltration and CAFs on antitumor therapy, we also explored the relationship between this prognostic model and immunotherapy response. We calculated the TIDE score to compare immunotherapy responses in the high-risk and low-risk groups. The high-risk group had higher TIDE and exclusion scores, which may be related to the levels of immune cell infiltration (*Figure 7D*). Thus, these results confirmed the correlation between this signature and TME

© Journal of Thoracic Disease. All rights reserved.

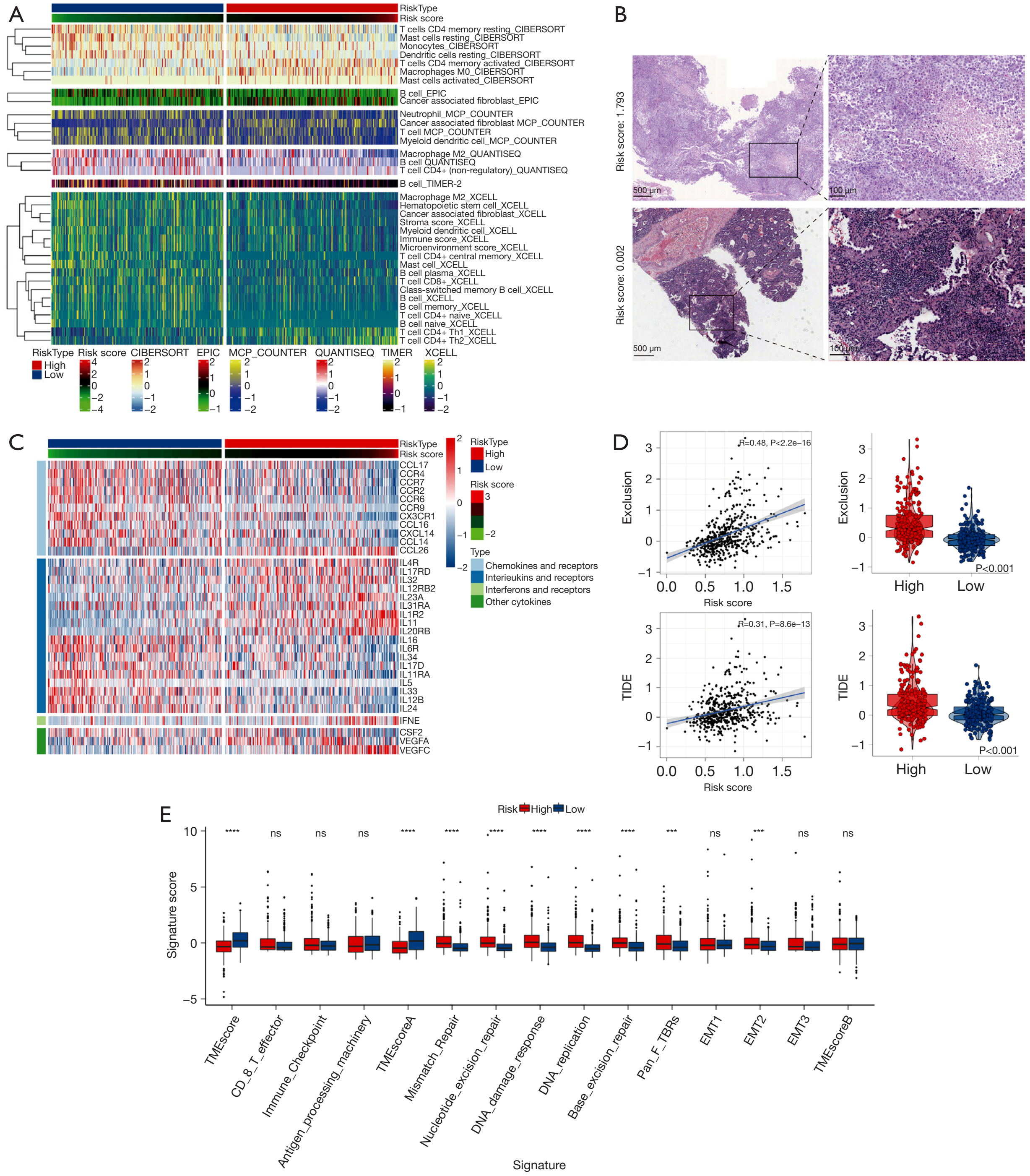

Figure 7 Differences in immune cell infiltration characteristics and immune-related gene expression in the different risk groups. (A) Heatmap showing the immune infiltration status for the different risk groups. (B) Representative images of pathological HE staining of patients with the highest and lowest risk scores in TCGA database (TCGA pathology slide). (C) Thermogram showing the mRNA expression levels of chemokines, interieukins, interferons, and other cytokines in the high- and low-risk groups. (D) Exclusion and TIDE scores for the different risk groups. (E) Box plot showing the TME-related scores in the different groups. The upper and lower ends of the box correspond to the quartile ranges of values, lines to medians, and dots to outliers. ns, P≥0.05; ***, P<0.001; ****, P<0.0001. TCGA, The Cancer Genome Atlas; TIDE, tumor immune dysfunction and exclusion; TME, tumor microenvironment; EMT, epithelial-mesenchymal transition; Pan-F-TBRs, pan-fibroblast TGF-β response signature; HE, hematoxylin eosin.

© Journal of Thoracic Disease. All rights reserved.

immune cell infiltration.

Moreover, we compared the immune-related gene set scores of the different risk groups. The high-risk group had higher scores for epithelial-mesenchymal transition 2 (EMT2), pan-fibroblast TGF-β response signature (Pan-F-TBRs), and DNA repair-related gene sets and lower scores for the TME score gene set (*Figure 7E*). Thus, the prognostic model was strongly correlated with the level of immune cell infiltration in the TME of patients with LUAD.

Discussion

The essential regulatory role of the TME in cancer development processes, such as cancer cell survival, growth, migration, and even dormancy, is well established (5). Within the TME, CAFs are the most highly represented nonneoplastic stromal cells, and their significant roles in tumor progression have been identified in recent years (39). CAFs play a significant role in tumor progression by secreting various factors, such as growth factors, extracellular matrix proteins, and immunosuppressive ligands, which also contribute to the immunosuppressive effects of the TME (40). In LUAD, CAFs promote cancer progression by enhancing glutamine uptake in LUAD cells through CAF-specific long-chain non-coding RNA LINC01614 packaged in secreted exosomes (41). Furthermore, the reduction of extracellular CLCN3 secretion via HNRNPK knockdown inhibits CAF activation and TGF-β1 production. This, in turn, affects the expression of nuclear HNRNPK and LUAD progression in a feedback loop (42). Due to the apparent heterogeneity of CAF markers, some studies have suggested that CAFs identified by a single or different marker may constitute various subtypes of CAFs with different functional roles in cancer progression. Haichuan Hu and colleagues identified three significant functional subtypes of CAFs in their study, based on distinct expression levels of hepatocyte growth factor (HGF), fibroblast growth factor 7 (FGF7), using PDF libraries. These subtypes exhibited diverse effects, particularly when treated with EGFR and ALK TKI (43). Therefore, reliable biomarkers based on CAFs have attracted an increasing amount of attention. However, CAF-related gene signatures in LUAD studies remain rare. Developing a gene signature based on CAFs in LUAD may help to understand how CAF relates to LUAD outcome, which could help classify patients and tailor therapies.

Recent applications of scRNA-seq have provided an objective characterization of TME cells and clear insights into the whole tumor ecosystem. In this study, we first confirmed that the proportion of CAFs in patients with LUAD was strongly correlated with survival and immune status in these patients. Next, using scRNA-seq analysis, we explored the CAF marker genes in LUAD that could not be distinguished in bulk RNA sequencing. Using the CAFs marker genes, we constructed a new prognostic signature for patients with LUAD in TCGA data set and validated it in 3 independent GEO cohorts and different clinical subgroups. We then confirmed that the signature was a reliable risk predictor. A comparison of the levels of enriched biological pathways and the immune cell infiltration of the high- and low-risk subgroups showed that the risk scores were positively correlated with the activation of oncogenic biological pathways and negatively correlated with the activation of immune-related pathways and levels of immune cell infiltration in the TME. In addition to tumor growth, invasion, and metastasis, CAFs also affect tumor treatment resistance (44). In gastric cancer, CAFs are able to secrete the exosome miR-522, which inhibits iron death in cancer cells by targeting ALOX15, thereby enhancing chemotherapy resistance (45). In HNSCC, CAFs are also involved in influencing the therapeutic efficacy of cetuximab, an effect that is strongly associated with TGF-β signaling (46). In this study, high-risk LUAD patients had higher TIDE and exclusion scores than did the low-risk patients, suggesting a higher immunotherapy response rate in the low-risk group. Further validation indicated that the signature could help determine LUAD prognosis, assess immune infiltration in the TME, and predict the effects of immunotherapy. An important research objective is to stratify the subgroup of high-risk patients with poor outcomes or low overall survival times after curative surgery for early-stage lung adenocarcinoma (LUAD). In this study, all the LUAD patients in the validation dataset (GSE30219) were at TNM stage I. Using the CAF-related signature developed in this study, we were able to categorize patients into high- and low-risk groups, which showed a significant difference in overall survival (P<0.0001). Therefore, we propose that this signature has the potential to identify a high-risk subgroup of early-stage LUAD patients, where the differential expression of the 11 genes involved in the signature may underlie the aggressive phenotype of early-stage LUAD.

The biological functions of the 11 CAF marker genes have been studied. Among them, *KRT8*, *FSTL3*, *ID1*, and *AKAP12* are associated with unfavorable outcomes. KRT8 is a type II basic intermediate filament protein; elevated

© Journal of Thoracic Disease. All rights reserved.

KRT8 levels have been reported in multiple human cancer types (47). *KRT8* has been further shown to enhance the proliferation, migration, and invasion ability of lung cancer cells and is significantly associated with survival in LUAD (48,49). *FSTL3*, an established oncogene, participates in the development and progression of NSCLC (50). Yang *et al.* confirmed that *FSTL3* activates EMT, promotes the polarization of macrophages and fibroblasts, and exhausts T cells (51). Moreover, a significant correlation was found between *FSTL3* expression and immune and stromal components of TMEs (51); this is in line with the findings related to our signature, which was strongly related to immune-related pathways and the level of immune cell infiltration. ID1 belongs to the helix-loop-helix (HLH) family and is a dominant negative regulator of transcription factors of the basic HLH family (52). As a direct downstream effector of the BMP/Smad pathway, ID1 has a proangiogenic effect. In addition, it exerts antitumor immunosuppressive effects by inhibiting dendritic cell differentiation and $CD8^+$ T cell proliferation (53,54). Baraibar *et al.* showed that programmed cell death protein 1 (PD-1) blockade combined with ID1 inhibition increased the infiltration of $CD8^+$ T cells and their programmed death-ligand 1 (PD-L1) expression, thereby significantly enhancing the immunotherapeutic effect (55). This result explains the lower $CD8^+$ T lymphocyte infiltration in the high-risk group. AKAP12 belongs to the kinase-anchored protein family (56). In LUAD, however, the role of *AKAP12* remains unclear. Chang *et al.* reported that *AKAP12* expression was upregulated in LUAD, and its high expression was related to tumor progression and poor prognosis (57).

The remaining 7 genes exerted beneficial impacts on the outcome of patients with LUAD. Although *FMO3* has rarely been studied in lung cancer, it does increase apoptosis and reduce cell viability in hepatocellular carcinoma cells (58). *BMP5* belongs to the transforming growth factor-β superfamily and participates in PinX1-related cell proliferation and cell cycle transition (59). Breast CAFs express the BMP antagonist *GREM1*, which promotes the mesenchymal phenotype, stemness, and invasion of cancer cells (60). Moreover, it is downregulated in LUAD and correlated with poor prognosis (61). *IGHM* is an immune-related gene encoding the C region of the μ heavy chain and defines its isoform (62). It significantly affects the density of infiltrating $CD20^+$ B cells in tumor tissues (63). In addition, Pocha *et al.* revealed that a high expression of surfactant genes, including *SFTPB*, was associated with intratumoral T-cell infiltration and a low immunosuppressive microenvironment in LUAD (64). As a xenobiotics metabolism enzyme, CYP4B1 has various biological roles. The *CYP4B1* mRNA level is low in LUAD and even lower in LUAD at advanced clinical stages (65,66). In lung cancer, *TMEM125* and *IRX2* have been studied less extensively. *IRX2* belongs to the Iroquois homeobox gene family, and there is evidence that LUADs commonly exhibit hypermethylation of the *IRX2* promoter region (67). In addition, Fan *et al.* developed a risk model based on transmembrane proteins, such as TMEM125, and explored its relationship with immune cell infiltration profiles in the TME (68). The specific mechanisms underlying the effects of *TMEM125* and *IRX* on the development of LUAD and its prognosis warrant further investigation.

We additionally examined the biological pathways associated with the CAF-related signature to better understand the mechanism underlying the effects of CAFs on LUAD. We found that common oncogenic pathways, including Hippo, Myc, PI3K, and Notch, as well as signaling pathways involved in cell cycle and DNA replication, were upregulated in the high-risk group. A previous study has reported that activating oncogenic pathways may inhibit immune infiltration (69). Furthermore, the Hippo pathway promotes cancer progression, and the main mediator of this pathway, yes-associated protein (YAP), participates in regulating PD-L1 expression in human NSCLC (70). Furthermore, Janse van Rensburg *et al.* reported that the Hippo signaling pathway targets PD-L1 and that transcriptional coactivator with PDZ-binding motif (TAZ), a Hippo pathway component, can promote immune evasion via PD-L1 (71). Meanwhile, Myc signaling can enable tumor cells to dysregulate their microenvironment and evade the host immune response (72,73). In addition, Isoyama *et al.* performed tumor immunotherapy combining a PI3K inhibitor and an anti-PD-1 monoclonal antibody, which suppressed T regulatory cell function and enhanced effector T cell function (74). Regarding the Notch signaling, numerous studies support its significance in immunotherapeutic efficacy (75,76). In agreement with these studies, we found that the following pathways were enriched in the low-risk group: antigen processing and presentation; cytokine–cytokine receptor interaction; and Th1, Th2, and Th17 cell differentiation. This finding prompted us to further investigate the relationship between this signature, the infiltration characteristics of the TME, and the response to immunotherapy.

The interaction of cancer cells and immune microenvironment components also regulate tumor growth and metastasis; thus, it is a crucial element for prognosis (77,78). We applied multiple algorithms to analyze the correlation between the signature and the immune cell infiltration characteristics. Our results show that the prognostic signature is significantly correlated to the immune cell infiltration characteristics in the TME. The low-risk group had higher levels of $CD8^+$ T cells, B cells, monocytes, neutrophils, and myeloid dendric cells than did the high-risk group. Tumor-infiltrating B cells have a distinct role in antitumor immunity. They can differentiate into plasma cells and produce antibodies that recognize tumor-associated antigens and generate antitumor responses (79). Dendric cells participate in antigen presentation, $CD4^+$ T cell differentiation, and natural killer cell recruitment; they are essential for efficient antitumor immunity (80). We also found that the high-risk group had higher infiltrating $CD4^+$ Th2 cell levels than did the low-risk group. In another study, the imbalance in the Th1:Th2 cell ratio was associated with overall survival in patients with lung cancer (81). Tumors with poor infiltration immune cells are described as "cold tumors" and are invariably associated with poor prognosis (78). Tumor-infiltrating lymphocytes are usually considered good prognostic tools—even superior to tumor stage in colon cancer (82). We compared the lymphocyte infiltration levels of the 2 risk groups using HE images of TCGA LUAD samples and confirmed that they were higher in the low-risk group, which may be one of the reasons for the better outcome in low-risk patients.

Cancer immunotherapies target the host immune response to fight the cancer. Because intratumoral $CD8^+$ T lymphocyte infiltration is critical to the success of immune checkpoint inhibitor therapy (83), we hypothesized that this prognostic signature could also help to predict the response to immune checkpoint inhibitor therapy in patients with LUAD. Using the TIDE algorithm, we found that high-risk patients had higher TIDE and exclusion scores, suggesting that immunotherapy is less effective in high-risk patients. Overall, low-risk patients had higher immune infiltration levels in the TME and reaped more benefits from immunotherapy.

This study has several limitations. First, it was based on a public data set, and confirming the predictive power of the obtained signature requires a large prospective clinical study. Second, the potential molecular mechanisms by which these CAF marker genes affect patient outcomes and immune infiltration need to be elucidated through further experimental studies.

Conclusions

We constructed and validated a prognostic signature based on 11 CAF marker genes by integrating scRNA and bulk RNA-seq analysis. In patients with LUAD, the signature could predict the outcome and immune infiltration characteristics well. Our study may provide a biomarker-based prognostic tool to predict outcome and immunotherapy impact, thus enhancing individualized treatment and improving prognosis.

Acknowledgments

We are very grateful to the GEO and TCGA databases for providing their platforms.
Funding: This research was funded by National Natural Science Foundation of China (No. 82172692).

Footnote

Reporting Checklist: The authors have completed the TRIPOD reporting checklist. Available at https://jtd.amegroups.com/article/view/10.21037/jtd-23-238/rc

Peer Review File: Available at https://jtd.amegroups.com/article/view/10.21037/jtd-23-238/prf

Conflicts of Interest: All authors have completed the ICMJE uniform disclosure form (available at https://jtd.amegroups.com/article/view/10.21037/jtd-23-238/coif). The authors have no conflicts of interest to declare.

Ethical Statement: The authors are accountable for all aspects of the work in ensuring that questions related to the accuracy or integrity of any part of the work are appropriately investigated and resolved. The study was conducted in accordance with the Declaration of Helsinki (as revised in 2013).

Open Access Statement: This is an Open Access article distributed in accordance with the Creative Commons Attribution-NonCommercial-NoDerivs 4.0 International License (CC BY-NC-ND 4.0), which permits the non-commercial replication and distribution of the article with the strict proviso that no changes or edits are made and the original work is properly cited (including links to both the

formal publication through the relevant DOI and the license). See: https://creativecommons.org/licenses/by-nc-nd/4.0/.

References

1. Sung H, Ferlay J, Siegel RL, et al. Global Cancer Statistics 2020: GLOBOCAN Estimates of Incidence and Mortality Worldwide for 36 Cancers in 185 Countries. CA Cancer J Clin 2021;71:209-49.
2. Thai AA, Solomon BJ, Sequist LV, et al. Lung cancer. Lancet 2021;398:535-54.
3. Herbst RS, Morgensztern D, Boshoff C. The biology and management of non-small cell lung cancer. Nature 2018;553:446-54.
4. Lin JJ, Cardarella S, Lydon CA, et al. Five-Year Survival in EGFR-Mutant Metastatic Lung Adenocarcinoma Treated with EGFR-TKIs. J Thorac Oncol 2016;11:556-65.
5. Bejarano L, Jordão MJC, Joyce JA. Therapeutic Targeting of the Tumor Microenvironment. Cancer Discov 2021;11:933-59.
6. Klemm F, Joyce JA. Microenvironmental regulation of therapeutic response in cancer. Trends Cell Biol 2015;25:198-213.
7. Binnewies M, Roberts EW, Kersten K, et al. Understanding the tumor immune microenvironment (TIME) for effective therapy. Nat Med 2018;24:541-50.
8. Chen Y, McAndrews KM, Kalluri R. Clinical and therapeutic relevance of cancer-associated fibroblasts. Nat Rev Clin Oncol 2021;18:792-804.
9. Mao X, Xu J, Wang W, et al. Crosstalk between cancer-associated fibroblasts and immune cells in the tumor microenvironment: new findings and future perspectives. Mol Cancer 2021;20:131.
10. Liu T, Han C, Wang S, et al. Cancer-associated fibroblasts: an emerging target of anti-cancer immunotherapy. J Hematol Oncol 2019;12:86.
11. Sato R, Imamura K, Semba T, et al. TGFβ Signaling Activated by Cancer-Associated Fibroblasts Determines the Histological Signature of Lung Adenocarcinoma. Cancer Res 2021;81:4751-65.
12. Lee S, Hong JH, Kim JS, et al. Cancer-associated fibroblasts activated by miR-196a promote the migration and invasion of lung cancer cells. Cancer Lett 2021;508:92-103.
13. Zhang H, Jiang H, Zhu L, et al. Cancer-associated fibroblasts in non-small cell lung cancer: Recent advances and future perspectives. Cancer Lett 2021;514:38-47.
14. Domen A, Quatannens D, Zanivan S, et al. Cancer-Associated Fibroblasts as a Common Orchestrator of Therapy Resistance in Lung and Pancreatic Cancer. Cancers (Basel) 2021;13:987.
15. Navab R, Strumpf D, Bandarchi B, et al. Prognostic gene-expression signature of carcinoma-associated fibroblasts in non-small cell lung cancer. Proc Natl Acad Sci U S A 2011; 108: 7160-7165.
16. Alcaraz J, Carrasco JL, Millares L, et al. Stromal markers of activated tumor associated fibroblasts predict poor survival and are associated with necrosis in non-small cell lung cancer. Lung Cancer 2019;135:151-60.
17. Yotsukura M, Asamura H, Suzuki S, et al. Prognostic impact of cancer-associated active fibroblasts and invasive architectural patterns on early-stage lung adenocarcinoma. Lung Cancer 2020;145:158-66.
18. Min K-W, Kim D-H, Noh Y-K, et al. Cancer-associated fibroblasts are associated with poor prognosis in solid type of lung adenocarcinoma in a machine learning analysis. Sci Rep 2021; 11: 16779.
19. Kim N, Kim HK, Lee K, et al. Single-cell RNA sequencing demonstrates the molecular and cellular reprogramming of metastatic lung adenocarcinoma. Nat Commun 2020;11:2285.
20. Wu F, Fan J, He Y, et al. Single-cell profiling of tumor heterogeneity and the microenvironment in advanced non-small cell lung cancer. Nat Commun 2021;12:2540.
21. Zhou Y, Yang D, Yang Q, et al. Single-cell RNA landscape of intratumoral heterogeneity and immunosuppressive microenvironment in advanced osteosarcoma. Nat Commun 2020;11:6322.
22. Maynard A, McCoach CE, Rotow JK, et al. Therapy-Induced Evolution of Human Lung Cancer Revealed by Single-Cell RNA Sequencing. Cell 2020;182:1232-1251.e22.
23. Song P, Li W, Wu X, et al. Integrated analysis of single-cell and bulk RNA-sequencing identifies a signature based on B cell marker genes to predict prognosis and immunotherapy response in lung adenocarcinoma. Cancer Immunol Immunother 2022;71:2341-54.
24. Racle J, Gfeller D. EPIC: A Tool to Estimate the Proportions of Different Cell Types from Bulk Gene Expression Data. Methods Mol Biol 2020;2120:233-48.
25. Hänzelmann S, Castelo R, Guinney J. GSVA: gene set variation analysis for microarray and RNA-seq data. BMC Bioinformatics 2013;14:7.
26. Hao Y, Hao S, Andersen-Nissen E, et al. Integrated analysis of multimodal single-cell data. Cell

2021;184:3573-3587.e29.

27. Aran D, Looney AP, Liu L, et al. Reference-based analysis of lung single-cell sequencing reveals a transitional profibrotic macrophage. Nat Immunol 2019;20:163-72.
28. Ritchie ME, Phipson B, Wu D, et al. limma powers differential expression analyses for RNA-sequencing and microarray studies. Nucleic Acids Res 2015;43:e47.
29. Xiao Y, Ma D, Zhao S, et al. Multi-Omics Profiling Reveals Distinct Microenvironment Characterization and Suggests Immune Escape Mechanisms of Triple-Negative Breast Cancer. Clin Cancer Res 2019;25:5002-14.
30. Yu G, Wang LG, Han Y, et al. clusterProfiler: an R package for comparing biological themes among gene clusters. OMICS 2012;16:284-7.
31. Newman AM, Liu CL, Green MR, et al. Robust enumeration of cell subsets from tissue expression profiles. Nat Methods 2015;12:453-7.
32. Becht E, Giraldo NA, Lacroix L, et al. Estimating the population abundance of tissue-infiltrating immune and stromal cell populations using gene expression. Genome Biol 2016;17:218.
33. Finotello F, Mayer C, Plattner C, et al. Molecular and pharmacological modulators of the tumor immune contexture revealed by deconvolution of RNA-seq data. Genome Med 2019;11:34.
34. Li B, Severson E, Pignon JC, et al. Comprehensive analyses of tumor immunity: implications for cancer immunotherapy. Genome Biol 2016;17:174.
35. Aran D, Hu Z, Butte AJ. xCell: digitally portraying the tissue cellular heterogeneity landscape. Genome Biol 2017;18:220.
36. Saltz J, Gupta R, Hou L, et al. Spatial Organization and Molecular Correlation of Tumor-Infiltrating Lymphocytes Using Deep Learning on Pathology Images. Cell Rep 2018;23:181-193.e7.
37. Charoentong P, Finotello F, Angelova M, et al. Pan-cancer Immunogenomic Analyses Reveal Genotype-Immunophenotype Relationships and Predictors of Response to Checkpoint Blockade. Cell Rep 2017;18:248-62.
38. Jiang P, Gu S, Pan D, et al. Signatures of T cell dysfunction and exclusion predict cancer immunotherapy response. Nat Med 2018;24:1550-8.
39. Hu B, Wu C, Mao H, et al. Subpopulations of cancer-associated fibroblasts link the prognosis and metabolic features of pancreatic ductal adenocarcinoma. Annals of Translational Medicine 2022; 10: 262.
40. Biffi G, Tuveson DA. Diversity and Biology of Cancer-Associated Fibroblasts. Physiol Rev 2021;101:147-76.
41. Liu T, Han C, Fang P, et al. Cancer-associated fibroblast-specific lncRNA LINC01614 enhances glutamine uptake in lung adenocarcinoma. J Hematol Oncol 2022;15:141.
42. Li Y, Yang Y, Ma Q, et al. HNRNPK/CLCN3 axis facilitates the progression of LUAD through CAF-tumor interaction. Int J Biol Sci 2022;18:6084-6101.
43. Hu H, Piotrowska Z, Hare PJ, et al. Three subtypes of lung cancer fibroblasts define distinct therapeutic paradigms. Cancer Cell 2021;39:1531-1547.e10.
44. Zhang J, Zhang N, Fu X, et al. Bioinformatic analysis of cancer-associated fibroblast related gene signature as a predictive model in clinical outcomes and immune characteristics of gastric cancer. Annals of Translational Medicine 2022;10:698.
45. Zhang H, Deng T, Liu R, et al. CAF secreted miR-522 suppresses ferroptosis and promotes acquired chemo-resistance in gastric cancer. Mol Cancer 2020;19:43.
46. Yegodayev KM, Novoplansky O, Golden A, et al. TGF-Beta-Activated Cancer-Associated Fibroblasts Limit Cetuximab Efficacy in Preclinical Models of Head and Neck Cancer. Cancers (Basel) 2020;12:339.
47. Fang J, Wang H, Liu Y, et al. High KRT8 expression promotes tumor progression and metastasis of gastric cancer. Cancer Sci 2017;108:178-86.
48. Chen H, Chen X, Pan B, et al. KRT8 Serves as a Novel Biomarker for LUAD and Promotes Metastasis and EMT via NF-κB Signaling. Front Oncol 2022;12:875146.
49. Xie L, Dang Y, Guo J, et al. High KRT8 Expression Independently Predicts Poor Prognosis for Lung Adenocarcinoma Patients. Genes (Basel) 2019;10:36.
50. Liu YJ, Li JP, Zhang Y, et al. FSTL3 is a Prognostic Biomarker in Gastric Cancer and is Correlated with M2 Macrophage Infiltration. Onco Targets Ther 2021;14:4099-117.
51. Yang C, Cao F, Huang S, et al. Follistatin-Like 3 Correlates With Lymph Node Metastasis and Serves as a Biomarker of Extracellular Matrix Remodeling in Colorectal Cancer. Front Immunol 2021;12:717505.
52. Perk J, Iavarone A, Benezra R. Id family of helix-loop-helix proteins in cancer. Nat Rev Cancer 2005;5:603-14.
53. Huang L, Zeng H, Jin C, et al. Sulfated galactoglucan impedes xenografted lung cancer cell growth by blocking angiogenesis via binding BMPRs. Carbohydr Polym 2022;289:119412.
54. Papaspyridonos M, Matei I, Huang Y, et al. Id1 suppresses

© Journal of Thoracic Disease. All rights reserved.

anti-tumour immune responses and promotes tumour progression by impairing myeloid cell maturation. Nat Commun 2015;6:6840.

55. Baraibar I, Roman M, Rodríguez-Remírez M, et al. Id1 and PD-1 Combined Blockade Impairs Tumor Growth and Survival of KRAS-mutant Lung Cancer by Stimulating PD-L1 Expression and Tumor Infiltrating CD8(+) T Cells. Cancers (Basel) 2020;12:3169.
56. Wu X, Wu T, Li K, et al. The Mechanism and Influence of AKAP12 in Different Cancers. Biomed Environ Sci 2018;31:927-32.
57. Chang J, Liu S, Li B, et al. MiR-338-3p improved lung adenocarcinoma by AKAP12 suppression. Arch Med Sci 2021;17:462-73.
58. Hlady RA, Sathyanarayan A, Thompson JJ, et al. Integrating the Epigenome to Identify Drivers of Hepatocellular Carcinoma. Hepatology 2019;69:639-52.
59. Xu Z, Chen C. Abnormal Expression and Prognostic Significance of Bone Morphogenetic Proteins and Their Receptors in Lung Adenocarcinoma. Biomed Res Int 2021;2021:6663990.
60. Ren J, Smid M, Iaria J, et al. Cancer-associated fibroblast-derived Gremlin 1 promotes breast cancer progression. Breast Cancer Res 2019;21:109.
61. Deng T, Lin D, Zhang M, et al. Differential expression of bone morphogenetic protein 5 in human lung squamous cell carcinoma and adenocarcinoma. Acta Biochim Biophys Sin (Shanghai) 2015;47:557-63.
62. Lee H, Kwon MJ, Koo BM, et al. A novel immune prognostic index for stratification of high-risk patients with early breast cancer. Sci Rep 2021;11:128.
63. Lu Z, Gao Y. Screening differentially expressed genes between endometriosis and ovarian cancer to find new biomarkers for endometriosis. Ann Med 2021;53:1377-89.
64. Pocha K, Mock A, Rapp C, et al. Surfactant Expression Defines an Inflamed Subtype of Lung Adenocarcinoma Brain Metastases that Correlates with Prolonged Survival. Clin Cancer Res 2020;26:2231-43.
65. Liu J, Jia J, Wang S, et al. Prognostic Ability of Enhancer RNAs in Metastasis of Non-Small Cell Lung Cancer. Molecules 2022;27:4108.
66. Zhang D, Jiang Q, Ge X, et al. RHOV promotes lung adenocarcinoma cell growth and metastasis through JNK/c-Jun pathway. Int J Biol Sci 2021;17:2622-32.
67. Sato T, Arai E, Kohno T, et al. Epigenetic clustering of lung adenocarcinomas based on DNA methylation profiles in adjacent lung tissue: Its correlation with smoking history and chronic obstructive pulmonary disease. Int J Cancer 2014;135:319-34.
68. Fan T, Liu Y, Liu H, et al. Transmembrane Protein-Based Risk Model and H3K4me3 Modification Characteristics in Lung Adenocarcinoma. Front Oncol 2022;12:828814.
69. Zhao X, Subramanian S. Oncogenic pathways that affect antitumor immune response and immune checkpoint blockade therapy. Pharmacol Ther 2018;181:76-84.
70. Hsu PC, Jablons DM, Yang CT, et al. Epidermal Growth Factor Receptor (EGFR) Pathway, Yes-Associated Protein (YAP) and the Regulation of Programmed Death-Ligand 1 (PD-L1) in Non-Small Cell Lung Cancer (NSCLC). Int J Mol Sci 2019;20:3821.
71. Janse van Rensburg HJ, Azad T, Ling M, et al. The Hippo Pathway Component TAZ Promotes Immune Evasion in Human Cancer through PD-L1. Cancer Res 2018;78:1457-70.
72. Schaafsma E, Zhao Y, Zhang L, et al. MYC Activity Inference Captures Diverse Mechanisms of Aberrant MYC Pathway Activation in Human Cancers. Mol Cancer Res 2021;19:414-28.
73. Dhanasekaran R, Deutzmann A, Mahauad-Fernandez WD, et al. The MYC oncogene - the grand orchestrator of cancer growth and immune evasion. Nat Rev Clin Oncol 2022;19:23-36.
74. Isoyama S, Mori S, Sugiyama D, et al. Cancer immunotherapy with PI3K and PD-1 dual-blockade via optimal modulation of T cell activation signal. J Immunother Cancer 2021;9:e002279.
75. Janghorban M, Xin L, Rosen JM, et al. Notch Signaling as a Regulator of the Tumor Immune Response: To Target or Not To Target? Front Immunol 2018;9:1649.
76. Sierra RA, Trillo-Tinoco J, Mohamed E, et al. Anti-Jagged Immunotherapy Inhibits MDSCs and Overcomes Tumor-Induced Tolerance. Cancer Res 2017;77:5628-38.
77. Remark R, Becker C, Gomez JE, et al. The non-small cell lung cancer immune contexture. A major determinant of tumor characteristics and patient outcome. Am J Respir Crit Care Med 2015;191:377-90.
78. Galon J, Bruni D. Approaches to treat immune hot, altered and cold tumours with combination immunotherapies. Nat Rev Drug Discov 2019;18:197-218.
79. Wang SS, Liu W, Ly D, et al. Tumor-infiltrating B cells: their role and application in anti-tumor immunity in lung cancer. Cell Mol Immunol 2019;16:6-18.
80. Wculek SK, Cueto FJ, Mujal AM, et al. Dendritic cells in cancer immunology and immunotherapy. Nat Rev Immunol 2020;20:7-24.
81. Basu A, Ramamoorthi G, Albert G, et al. Differentiation

and Regulation of T(H) Cells: A Balancing Act for Cancer Immunotherapy. Front Immunol 2021;12:669474.

82. Galon J, Mlecnik B, Bindea G, et al. Towards the introduction of the 'Immunoscore' in the classification of malignant tumours. J Pathol 2014;232:199-209.

83. Rosenbaum SR, Wilski NA, Aplin AE. Fueling the Fire: Inflammatory Forms of Cell Death and Implications for Cancer Immunotherapy. Cancer Discov 2021;11:266-81.

(English Language Editor: J. Gray)

Cite this article as: Huang X, Xiao H, Shi Y, Ben S. Integrating single-cell and bulk RNA sequencing to develop a cancer-associated fibroblast-related signature for immune infiltration prediction and prognosis in lung adenocarcinoma. J Thorac Dis 2023;15(3):1406-1425. doi: 10.21037/jtd-23-238

© Journal of Thoracic Disease. All rights reserved.

Table S1 Marker gene sets for five carcinogenic pathways

Symbol	Pathway
CCND1	Cell.Cycle_activated
CCND2	Cell.Cycle_activated
CCND3	Cell.Cycle_activated
CCNE1	Cell.Cycle_activated
CDK2	Cell.Cycle_activated
CDK4	Cell.Cycle_activated
CDK6	Cell.Cycle_activated
E2F1	Cell.Cycle_activated
E2F3	Cell.Cycle_activated
YAP1	Hippo_activated
TEAD1	Hippo_activated
TEAD2	Hippo_activated
TEAD3	Hippo_activated
TEAD4	Hippo_activated
WWTR1	Hippo_activated
MYC	MYC_activated
MYCL1	MYC_activated
MYCN	MYC_activated
CREBBP	NOTCH_activated
EP300	NOTCH_activated
HES1	NOTCH_activated
HES2	NOTCH_activated
HES3	NOTCH_activated
HES4	NOTCH_activated
HES5	NOTCH_activated
HEY1	NOTCH_activated
HEY2	NOTCH_activated
HEYL	NOTCH_activated
KAT2B	NOTCH_activated
NOTCH1	NOTCH_activated
NOTCH2	NOTCH_activated
NOTCH3	NOTCH_activated
NOTCH4	NOTCH_activated
PSEN2	NOTCH_activated
LFNG	NOTCH_activated
NCSTN	NOTCH_activated
JAG1	NOTCH_activated
APH1A	NOTCH_activated
FHL1	NOTCH_activated
THBS2	NOTCH_activated
MFAP2	NOTCH_activated
RFNG	NOTCH_activated
MFAP5	NOTCH_activated
JAG2	NOTCH_activated
MAML3	NOTCH_activated
MFNG	NOTCH_activated
CNTN1	NOTCH_activated
MAML1	NOTCH_activated
MAML2	NOTCH_activated
PSEN1	NOTCH_activated
PSENEN	NOTCH_activated
RBPJ	NOTCH_activated
RBPJL	NOTCH_activated
SNW1	NOTCH_activated
ADAM10	NOTCH_activated
APH1B	NOTCH_activated
ADAM17	NOTCH_activated
DLK1	NOTCH_activated
DLL1	NOTCH_activated
DLL3	NOTCH_activated
DLL4	NOTCH_activated
DNER	NOTCH_activated
DTX1	NOTCH_activated
DTX2	NOTCH_activated
DTX3	NOTCH_activated
DTX3L	NOTCH_activated
DTX4	NOTCH_activated
EGFL7	NOTCH_activated
EIF4EBP1	PI3K_activated
AKT1	PI3K_activated
AKT2	PI3K_activated
AKT3	PI3K_activated
AKT1S1	PI3K_activated
INPP4B	PI3K_activated
MAPKAP1	PI3K_activated
MLST8	PI3K_activated
MTOR	PI3K_activated
PDK1	PI3K_activated
PIK3CA	PI3K_activated
PIK3CB	PI3K_activated
PIK3R2	PI3K_activated
RHEB	PI3K_activated
RICTOR	PI3K_activated
RPTOR	PI3K_activated
RPS6	PI3K_activated
RPS6KB1	PI3K_activated
STK11	PI3K_activated
CDKN1A	Cell.Cycle_repressed
CDKN1B	Cell.Cycle_repressed
CDKN2A	Cell.Cycle_repressed
CDKN2B	Cell.Cycle_repressed
CDKN2C	Cell.Cycle_repressed
RB1	Cell.Cycle_repressed
STK4	Hippo_repressed
STK3	Hippo_repressed
SAV1	Hippo_repressed
LATS1	Hippo_repressed
LATS2	Hippo_repressed
MOB1A	Hippo_repressed
MOB1B	Hippo_repressed
PTPN14	Hippo_repressed
NF2	Hippo_repressed
WWC1	Hippo_repressed
TAOK1	Hippo_repressed
TAOK2	Hippo_repressed
TAOK3	Hippo_repressed
CRB1	Hippo_repressed
CRB2	Hippo_repressed
CRB3	Hippo_repressed
LLGL1	Hippo_repressed
LLGL2	Hippo_repressed
HMCN1	Hippo_repressed
SCRIB	Hippo_repressed
HIPK2	Hippo_repressed
FAT1	Hippo_repressed
FAT2	Hippo_repressed
FAT3	Hippo_repressed
FAT4	Hippo_repressed
DCHS1	Hippo_repressed
DCHS2	Hippo_repressed
CSNK1E	Hippo_repressed
CSNK1D	Hippo_repressed
AJUBA	Hippo_repressed
LIMD1	Hippo_repressed
WTIP	Hippo_repressed
MGA	MYC_repressed
MNT	MYC_repressed
MXD1	MYC_repressed
MXD3	MYC_repressed
MXD4	MYC_repressed
MXI1	MYC_repressed
ARRDC1	NOTCH_repressed
CNTN6	NOTCH_repressed
KDM5A	NOTCH_repressed
NOV	NOTCH_repressed
NRARP	NOTCH_repressed
ITCH	NOTCH_repressed
SPEN	NOTCH_repressed
FBXW7	NOTCH_repressed
HDAC2	NOTCH_repressed
CUL1	NOTCH_repressed
NCOR1	NOTCH_repressed
NCOR2	NOTCH_repressed
HDAC1	NOTCH_repressed
NUMB	NOTCH_repressed
CIR1	NOTCH_repressed
NUMBL	NOTCH_repressed
RBX1	NOTCH_repressed
SAP30	NOTCH_repressed
SKP1	NOTCH_repressed
CTBP1	NOTCH_repressed
CTBP2	NOTCH_repressed
DEPDC5	PI3K_repressed
DEPTOR	PI3K_repressed
NPRL2	PI3K_repressed
NPRL3	PI3K_repressed
PIK3R1	PI3K_repressed
PIK3R3	PI3K_repressed
PPP2R1A	PI3K_repressed
PTEN	PI3K_repressed
TSC1	PI3K_repressed
TSC2	PI3K_repressed

Table S2 The list of 129 immunomodulators used in this study

Chemokines	Interleukins	Interferons	Other cytokines
CXCL10	IL21R	IFNG	IDO1
CCL11	IL12B	IFNB1	LTA
CXCL13	IL21	IFNAR2	FASLG
CXCL9	IL9R	IFNGR2	TNF
CXCL11	IL26	IFNA8	CSF2
CCR8	IL27	IFNA1	CSF2RB
CCL17	IL29	IFNE	CSF2RA
CCL20	IL2RB	IFNA5	VEGFA
CCR4	IL12RB1		TGFBR1
CCL18	IL10		FAS
CCL25	IL24		TGFB3
CXCR4	IL7R		CSF1
CXCR3	IL18		PDGFC
CCL26	IL32		ARG1
CCR3	IL2RG		VEGFC
CCR7	IL8		VEGFB
CCR5	IL2RA		PDGFRB
CCR2	IL12RB2		TGFBR2
XCL2	IL1A		PDGFRA
CCL5	IL22		EPOR
CCL4	IL10RA		PDGFA
CCR6	IL23A		CSF3
CCR1	IL31RA		EGFR
CCL3	IL1R2		PDGFD
CCL22	IL28A		EGF
CCL8	IL28B		TPO
XCL1	IL1B		TGFBR3
CXCR6	IL27RA		
CCL1	IL11		
CXCL16	IL20RB		
CXCR1	IL12A		
CXCR2	IL16		
CCR9	IL10RB		
PF4	IL6R		
CXCL6	IL10RB		
CX3CL1	IL6R		
CCR10	IL3RA		
CX3CR1	IL4R		
CXCR7	IL1R1		
CCL16	IL34		
CXCL14	IL17D		
CXCL12	IL6		
CCL21	IL11RA		
PPBP	IL5		
CCL14	IL17RD		
CCL28	IL33		
	IL20RA		
	IL17B		

© Journal of Thoracic Disease. All rights reserved.

https://dx.doi.org/10.21037/jtd-23-238

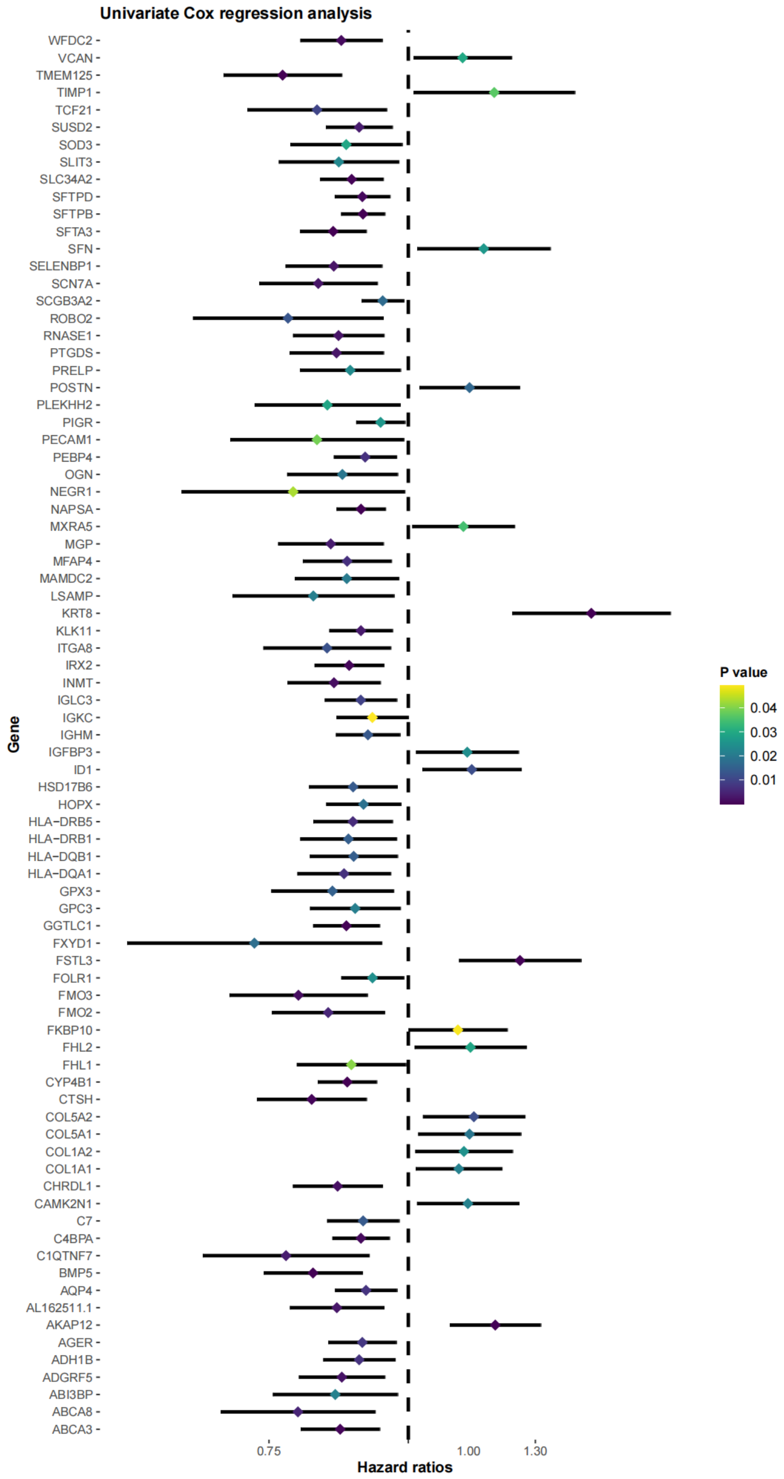

Figure S1 Forest plot of survival-associated genes obtained with univariate Cox analysis.

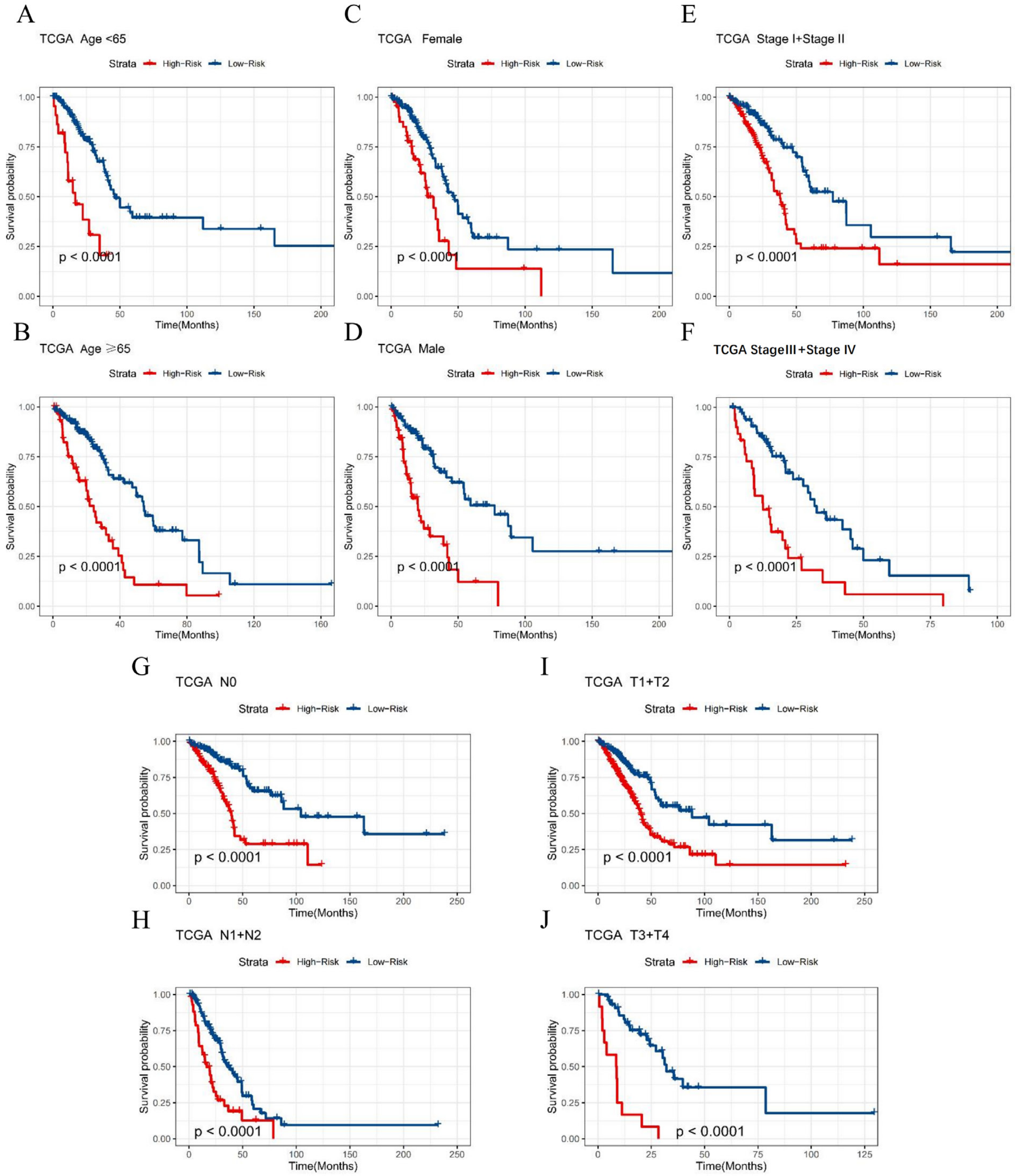

Figure S2 Validation of the prediction power of the signature in different subgroups of the TCGA cohort based on clinical variables. Kaplan-Meier overall survival analysis based on risk scores in TCGA database for the following subgroups: (A) aged <65 years, (B) aged ≥65 years, (C) female, (D) male, (E) at early stages (I + II), (F) at advanced stages (III + IV), (G) without lymph node metastasis, (H) with lymph node metastasis, (I) at early T stages (T1 + T2), and (J) at advanced T stages (T3 + T4). TCGA, The Cancer Genome Atlas.

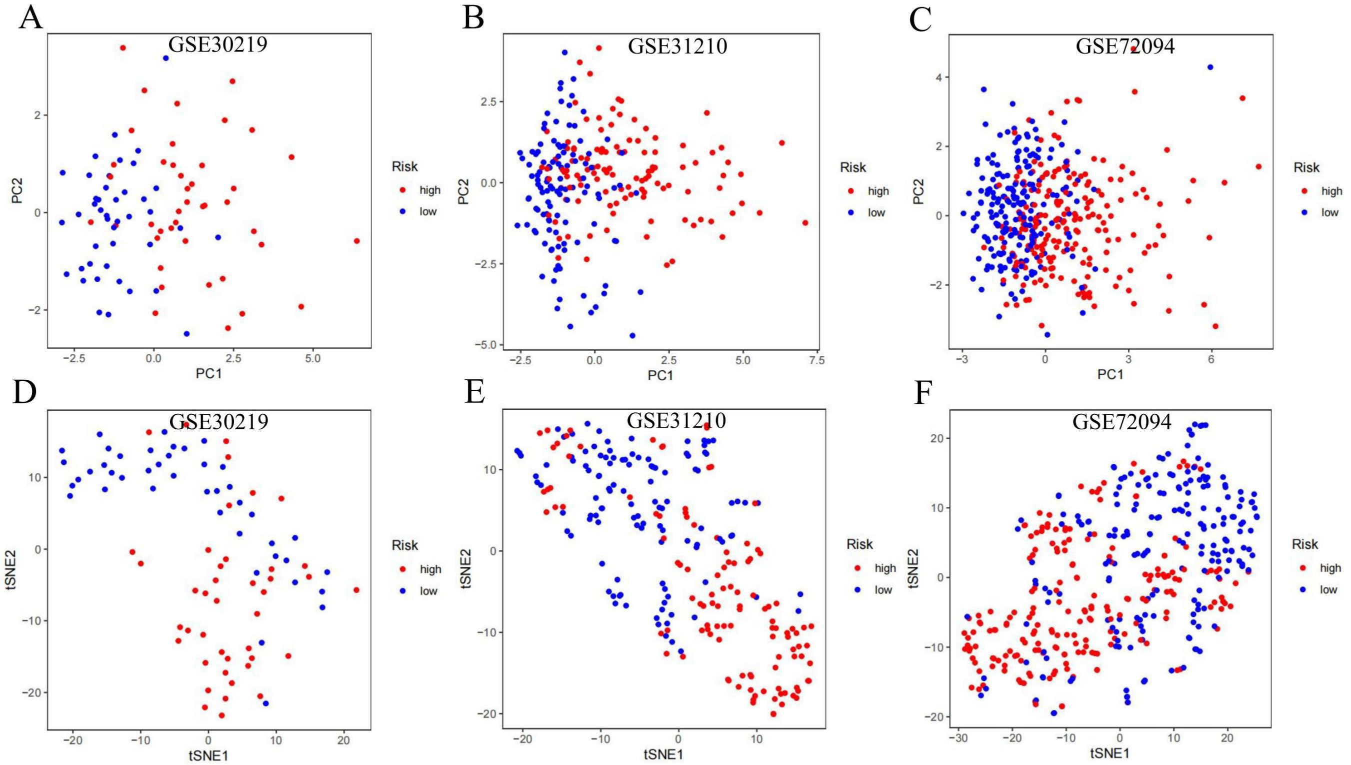

Figure S3 The PCA and tSNE analysis in the 3 validation cohorts. (A-C) PCA analysis and (D-F) tSNE analysis in the GSE30219, GSE31210, and GSE72094 cohorts. PCA, principal component analysis; tSNE, t-distributed stochastic neighbor embedding.

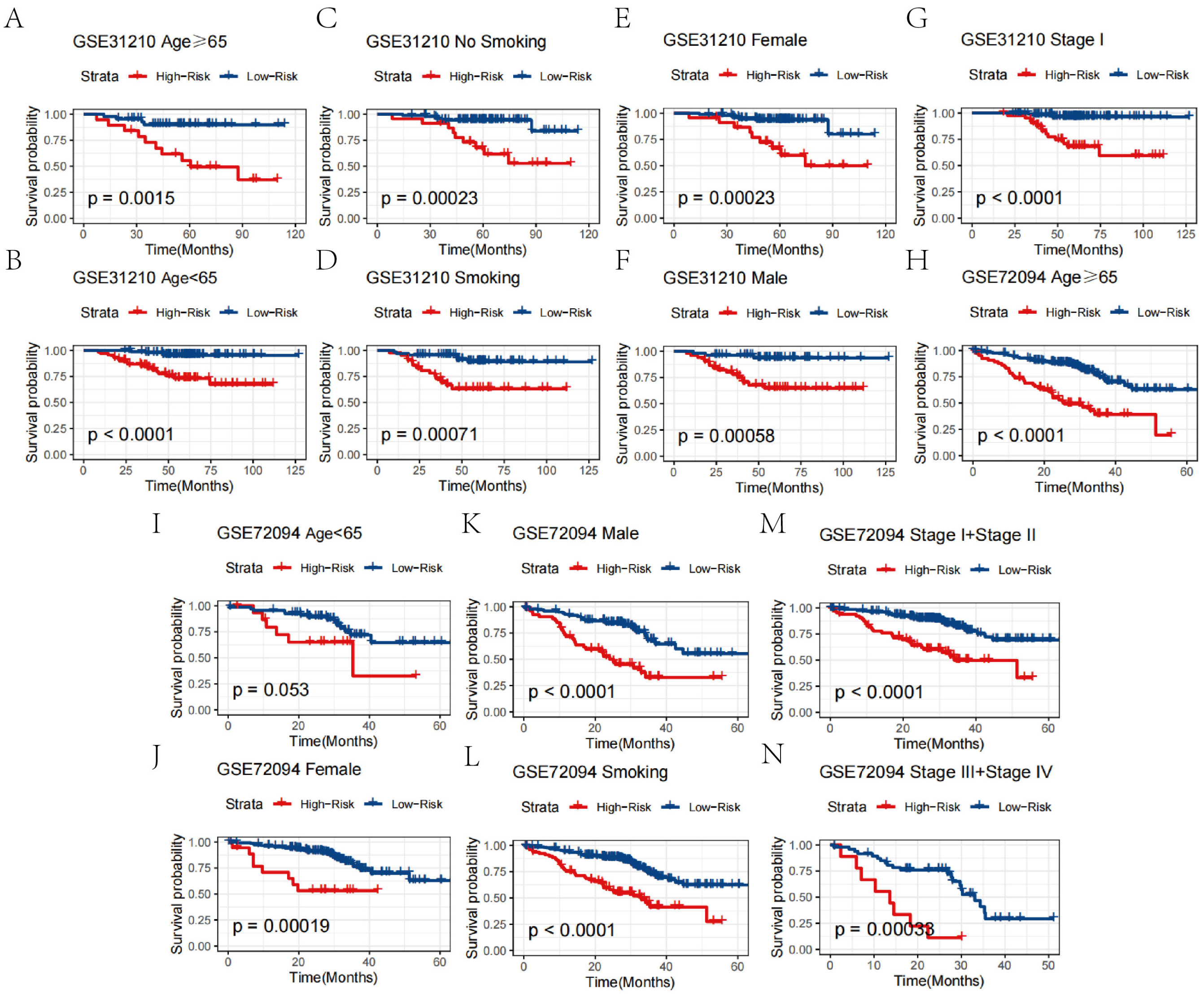

Figure S4 Validation of the prediction power of the signature in different subgroups of the GEO cohorts based on clinical variables. Kaplan-Meier overall survival analysis of the GSE31210 cohort for the following subgroups:(A) aged ≥65 years, (B) aged <65 years, (C) non-smoking, (D) smoking, (E) female, (F) male, and (G) at stage I. Kaplan-Meier overall survival curves based on risk score in the GSE72094 cohort for the following subgroups: (H) aged ≥65 years, (I) aged <65 years, (J) female, (K) male, (L) smoking, (M) at early stages (I + II), and (N) at advanced stages (III + IV). GEO, Gene Expression Omnibus.

© Journal of Thoracic Disease. All rights reserved.
https://dx.doi.org/10.21037/jtd-23-238

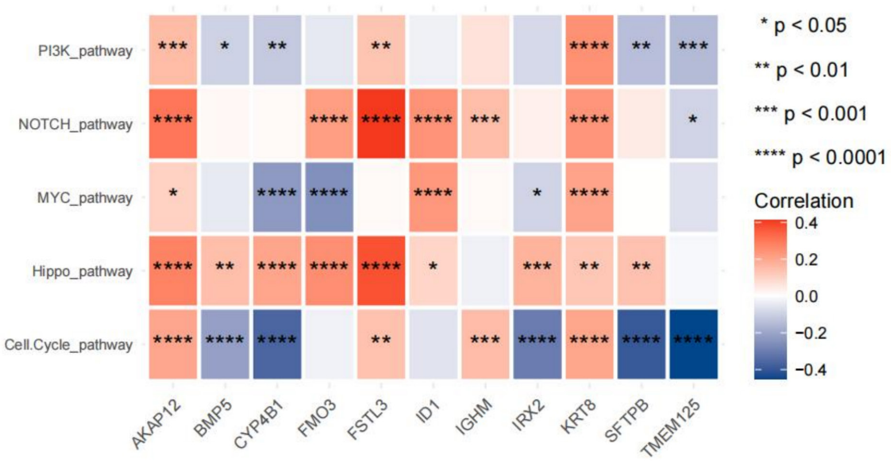

Figure S5 The thermogram shows the association between the 5 oncogenic signaling pathways and the 11 CAF marker genes.

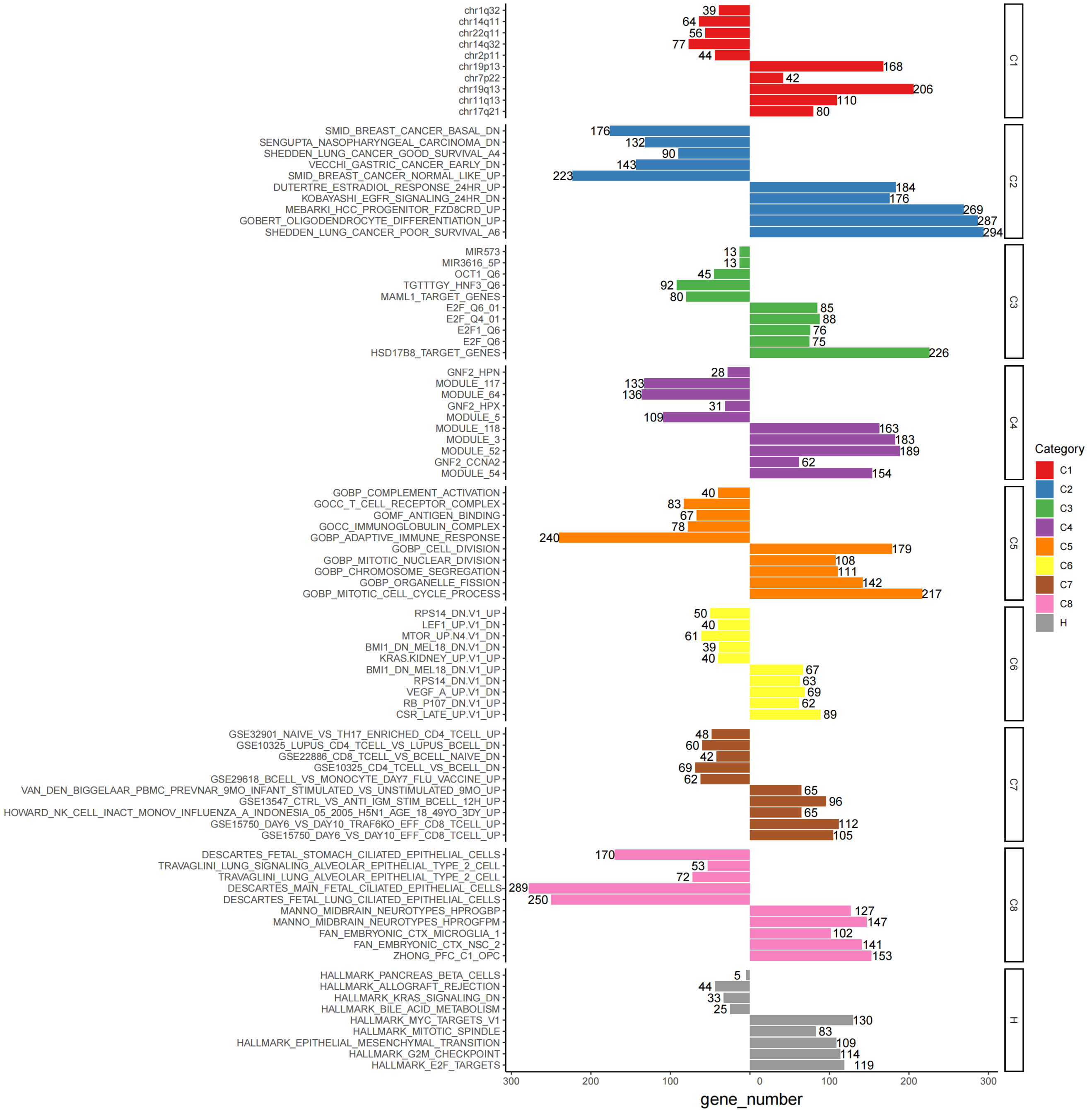

Figure S6 Histogram of gene set enrichment analysis based on MsigDB.

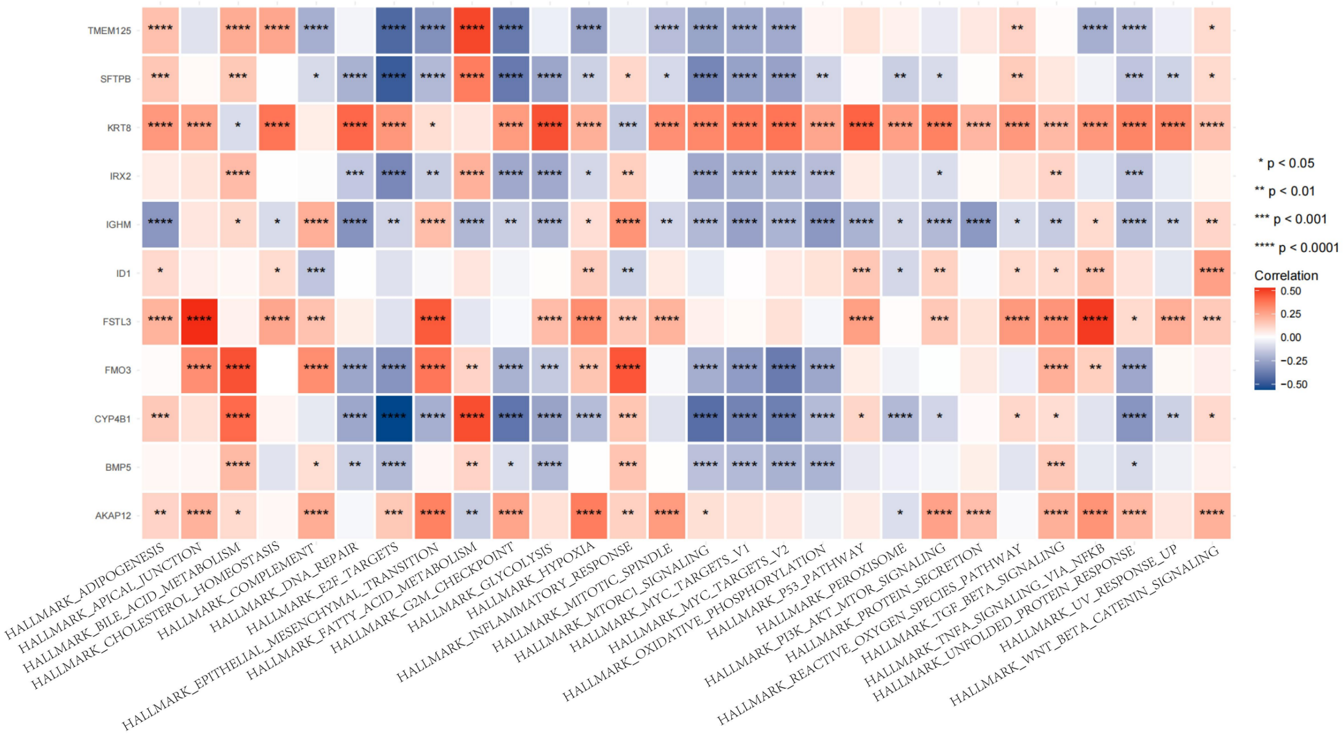

Figure S7 Thermogram showing the association between the marker genes and biological signaling pathways according to GSVA. CAF, cancer-associated fibroblast; GSVA, gene set variation analysis.

© Journal of Thoracic Disease. All rights reserved. https://dx.doi.org/10.21037/jtd-23-238

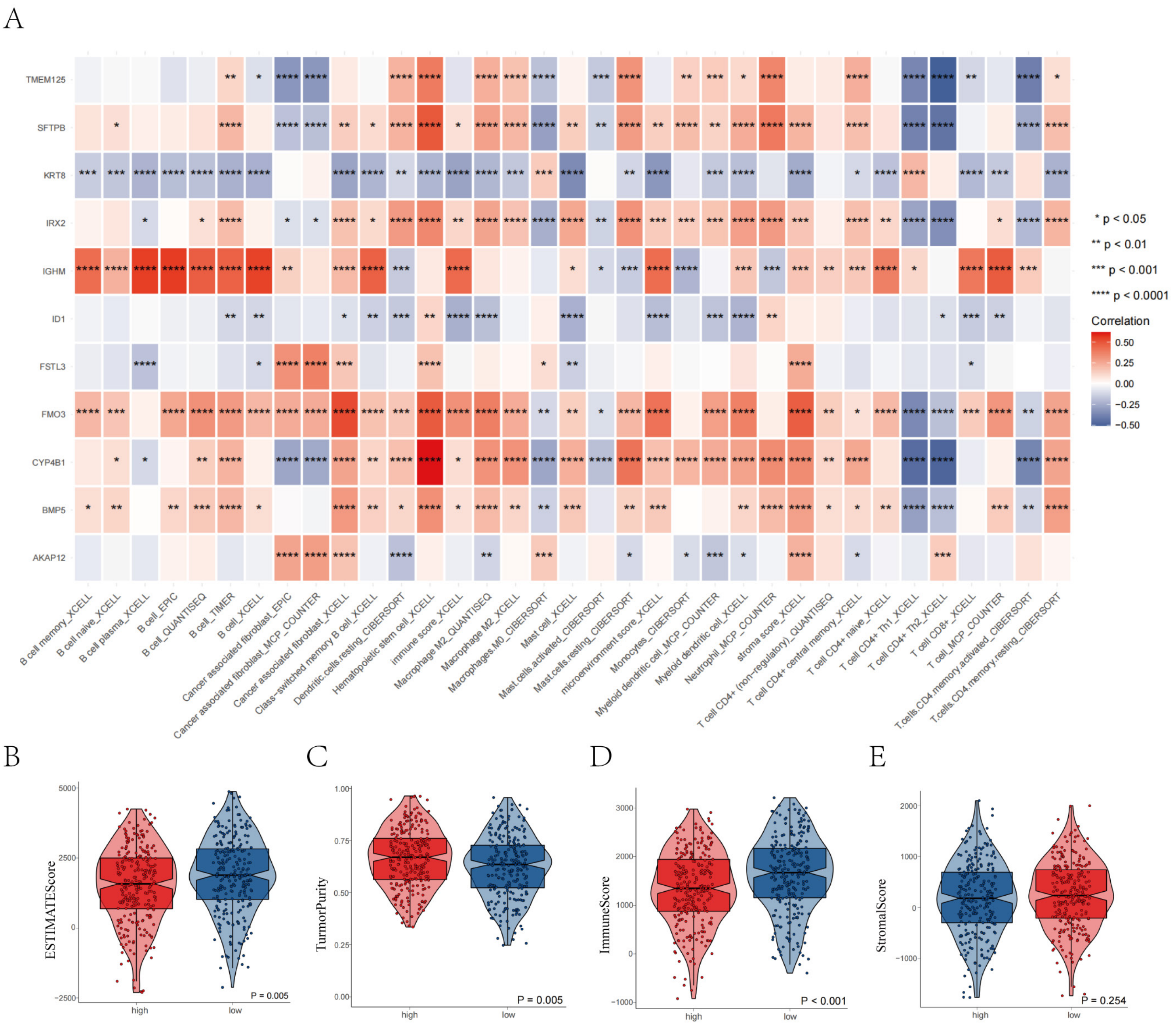

Figure S8 Correlation between the signature and immune cell infiltration in the TME. (A) Heatmap showing the correlation of the 11 CAF marker genes with immune cell infiltration characteristics. (B) Comparison of ESTIMATE scores, (C) tumor purity scores, (D) immune scores, and (E) stromal scores of the high-risk and low-risk groups. CAF, cancer-associated fibroblast; TME, the tumor microenvironment.

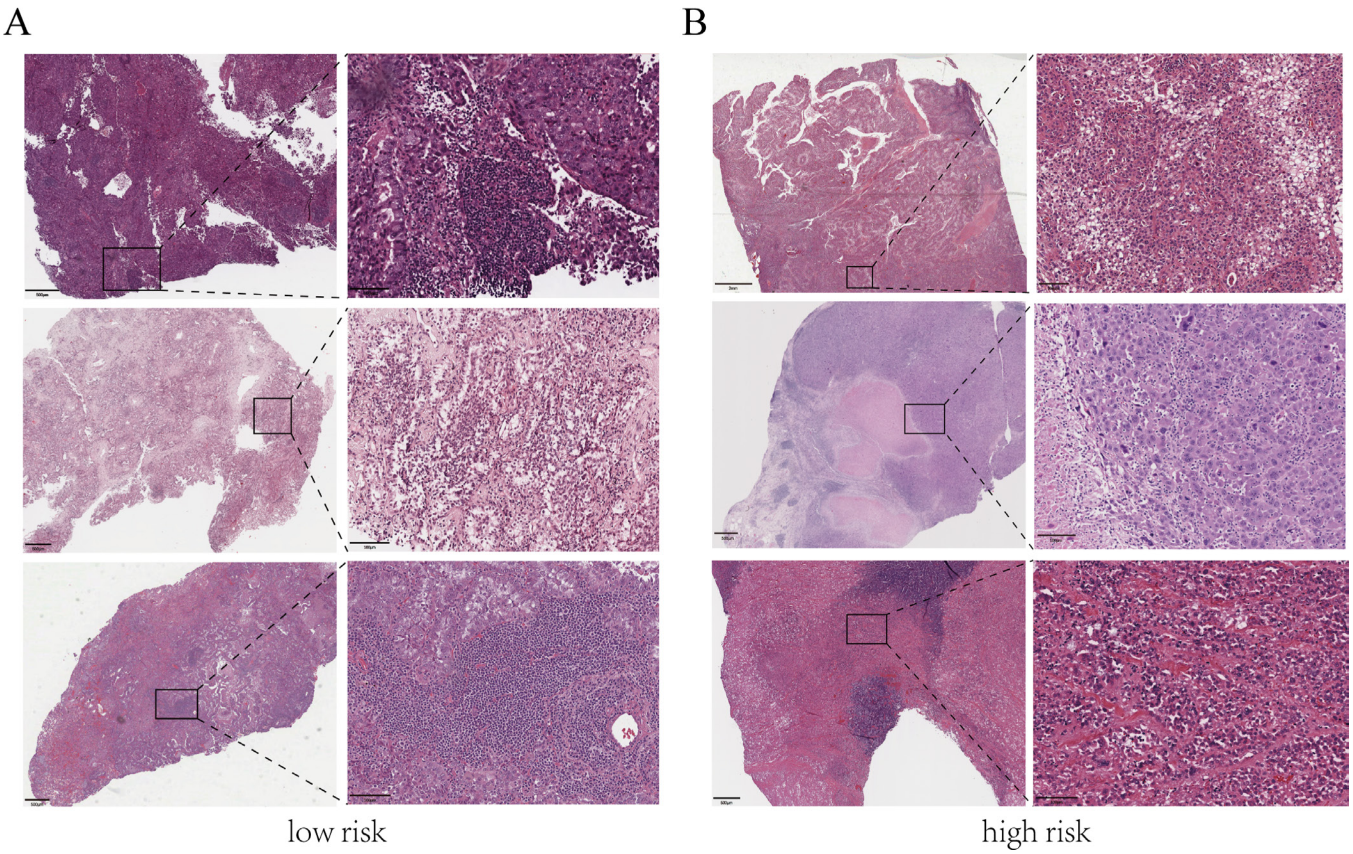

Figure S9 Representative images of HE staining of the (A) low-risk and (B) high-risk patients in TCGA database (TCGA pathology slides). HE staining, hematoxylin-eosin staining; TCGA, The Cancer Genome Atlas.